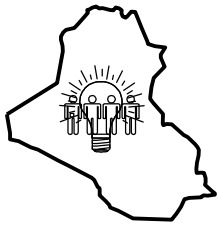

SPONSORED AND PUBLISHED BY
THE IRAQI SOCIETY FOR ALTERNATIVE AND RENEWABLE ENERGY SOURCES AND TECHNIQUES (I.S.A.R.E.S.T.)

EDITORIAL BOARD

ADVISORY BOARD

ORGANIZED BY I.S.A.R.E.S.T.

The **I**raqi **S**ociety for **A**lternative and **R**enewable **E**nergy **S**ources and **T**echniques (**I.S.A.R.E.S.T.**) will organize the following activities during this semester at the dates and places indicated:

SCIENTIFIC LECTURE

Date: 5th April 2005
Time: 11:00 am
Title: **Recent Developments in IR Detectors and Applications.**
Lecturer: **Dr. Raid A. Ismail (**Ministry of Science and Technology**)**
Place: Al-Khawarizmi Hall, School of Applied Sciences, University of Technology, Baghdad.

SCIENTIFIC LECTURE

Date: 19th April 2005
Time: 11:00 am
Title: **Optical Fiber Sensors (OFS's) and Applications.**
Lecturer: **Dr. Walid K. Hamoudi (**School of Applied Sciences, University of Technology, Baghdad.**)**
Place: Al-Khawarizmi Hall, School of Applied Sciences, University of Technology, Baghdad.

WORKSHOP

Date: 4th May 2005
Time: 11:00 am
Title: **The Optical Sources and Technologies**
Lecturers: **Dr. Walid K. Hamoudi** (Laser sources and their applications)
Dr. Raid A. Ismail (Solar energy sources)
Dr. Raad A. Khamis (Nuclear and plasma sources)
Place: Al-Khawarizmi Hall, School of Applied Sciences, University of Technology, Baghdad.

SCIENTIFIC LECTURE

Date: 18th May 2005
Time: 11:00 am
Title: **The Magnetized Waters and Their Applications**
Lecturer: **Dr. Raad A. Khamis (**School of Applied Sciences, University of Technology, Baghdad.**)**
Place: Al-Khawarizmi Hall, School of Applied Sciences, University of Technology, Baghdad.

SYMPOSIUM

Date: 22nd June 2005
Title: **Solar Energy Techniques and Their Employment in Iraq**
Place: Al-Khawarizmi Hall, School of Applied Sciences, University of Technology, Baghdad.

SCIENTIFIC LECTURE

Date: 29th June 2005
Time: 11:00 am
Title: **Detection of the Earth Magnetic Fields by Josephson Junction.**
Lecturer: **Dr. Dayah N. Raouf (**School of Applied Sciences, University of Technology, Baghdad.**)**
Place: Al-Khawarizmi Hall, School of Applied Sciences, University of Technology, Baghdad.

SCIENTIFIC LECTURE

Date: 6th July 2005
Time: 11:00 am
Title: **Semiconductor Nanocrystallites Production.**
Lecturer: **Dr. Bassam G. Rasheed (**School of Applied Sciences, University of Technology, Baghdad.**)**
Place: Al-Khawarizmi Hall, School of Applied Sciences, University of Technology, Baghdad.

Iraqi J. of Appl. Phys. , Vol. 1 , No. 2 , 2005 , 3-11

Michael J. Adams[(1)]
Donald A. Davies[(2)]
Michael C. Tatham[(2)]
Mil A. Fisher[(2)]

[(1)] *Electronic Systems Engineering Department, University of Essex, Wivenhoe Park, Colchester, Essex CO4 3SQ, UK*
[(2)] *BT laboratories, Martlesham, Ipswich IP5 7RE, UK*

Key Mechanisms of The Nonlinear Amplification: Physics and Applications

This review discusses the physical mechanisms of absorptive and dispersive nonlinearity in amplifiers resulting from interband and intraband electron transitions, with as assessment of the relative strengths and response times of these nonlinearities. Where appropriate, the potential applications of these nonlinearities in optical networks are also indicated.

Keywords: *Nonlinear amplification, Semiconductor lasers, Optical bistability, Wavelength conversion, Optical networks*

Received: 1 March 2005

1. Introduction

There has been considerable recent progress in the exploitation of optical nonlinearities in laser amplifiers. A range of potential applications has been identified, including wavelength conversion, optical demultiplexing, clock recovery, time and space switching, and dispersion compensation. It is anticipated that many of these optics will be of increasing importance in simplifying the architectural requirements for the optical networks of the twenty-first century. With this interest in mind, the objective of the present contribution is to review the topic of nonlinear laser amplifiers and to give an account of the physical mechanisms involved, in so far as they are understood at present. In order to address this objective it is convenient to categorize the nonlinearities as interband (i.e. associated with changes in electron concentrations in the conduction and valence bands) and intraband (i.e. due to changes in the energy distributions of electrons rather than in their numbers). By categorizing the effects in this way, recent dramatic advances (e.g. wavelength conversion and clock recovery at $20Gbs^{-1}$, all-optical multiplexing at bit rates of $40Gbs^{-1}$, $50Gbs^{-1}$ and $250Gbs^{-1}$) can be set in the historical context of previous development.

2. Interband nonlinearities

2.1 Saturation of gain/loss

Consider an intense optical beam incident on a semiconductor with a photon energy slightly greater than the band gap. The beam will be absorbed by electron transitions between the valence and conduction bands. If the beam is sufficiently intense then the absorption will be saturated since there will be a limited number of conduction band states where the transitions terminate. If the passive semiconductor is replaced by a semiconductor laser amplifier, so that the incident beam is amplified rather than absorbed, then saturation of the amplification will occur in an analogous fashion (there will be a limited number of states that can participate in transitions giving rise to optical gain). Thus for both active and passive systems this saturation can be described as a band-filling nonlinearity.

A simple analytical description of the saturation of either absorption or gain can be obtained from the steady-state rate equations for electrons and photons, assuming the recombination process to be characterized by a lifetime τ. denoting the saturated and unsaturated absorption (gain) coefficient per unit length as g and g_0, respectively, and assuming that the coefficient is linearly related to the electron concentration, we find [1]

$$\frac{g_0}{g} = 1 + \frac{P}{P_{sat}} \qquad (1)$$

where P is the incident power and P_{sat} is a saturation power given by

$$P_{sat} = \frac{EA}{\Gamma \tau (dg/dn)} \qquad (2)$$

In Equation 2, E denotes the photon energy, A the cross-sectional area of the sample (or the wavelength in a laser amplifier), Γ the confinement factor (cross-sectional fraction of power confined to the absorbing/amplifying region), and dg/dn the differential gain (n is the electron concentration). For example, in a laser amplifier of InGaAsP operating in the 1.55μm

wavelength range, typical values are E=0.8eV, A=0.3μm^2, Γ=0.3, τ=1ns, and dg/dn=2.5x10^{-16}cm^2, giving P_{sat}=5mW.

2.2 Two-section laser amplifiers

The idea of using saturable absorption as a switching mechanism in a semiconductor laser is almost as old as the laser itself. Two-section laser shown schematically in Fig. 1 was proposed by Lasher in 1964 [2] as a bistable device exhibiting hysteresis in the light-current characteristics. This behaviour is indeed observed experimentally, but the same device can also exhibit self-sustained pulsations caused by repetitive Q-switching via the saturable absorber [3]. In addition, when biased slightly below the threshold for light-current bistability, a device containing one or more saturable absorbers can exhibit switching and bistable operation by optical injection [4].

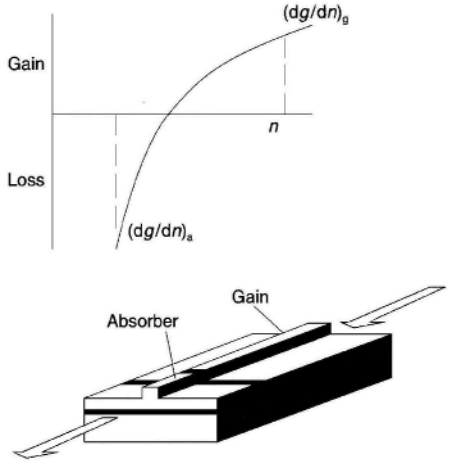

Fig.(1): The two-section laser amplifier. Inset: gain versus carrier concentration (schematic)

The conditions for stable, bistable and unstable operation have been investigated by many authors, but perhaps the most comprehensive theory has been given by Ueno and Lang [5]. Their results show that the stability conditions are determined by the lifetimes in the gain and absorbing sections (τ_g and τ_a, respectively) and the corresponding differential gains in these sections, denoted here by $(\mathrm{d}g/\mathrm{d}n)_g$ and $(\mathrm{d}g/\mathrm{d}n)_a$, respectively. Note that the differential gains are different as a consequence of the nonlinear gain-carrier density relation illustrated in the inset of Fig. 1. The condition for bistable behaviour is given by [5]

$$\tau_g\left(\frac{dg}{dn}\right)_g < \tau_a\left(\frac{dg}{dn}\right)_a C_1 \qquad (3)$$

where C_1 is a constant related to the relative lengths of absorber and gain sections, as well as other device parameters. The conditions for unstable behaviour are

$$\tau_g\left(\frac{dg}{dn}\right)_g > \tau_a\left(\frac{dg}{dn}\right)_a C_1 \quad \text{and}$$

$$\tau_g\left(\frac{dg}{dn}\right)_a < \tau_a\left(\frac{dg}{dn}\right)_g C_2 \qquad (4)$$

where C_2 is another constant similar to C_1 (note that Equation 4 differs slightly from the result given in [5], and has been derived by a modified treatment [6]). Figure 2 shows the regions of stable, unstable and bistable behaviour in the τ_g/τ_a-$(\mathrm{d}g/\mathrm{d}n)_g/(\mathrm{d}g/\mathrm{d}n)_a$ plane, as described by Equations 3 and 4. the unstable region contains areas where self-pulsation can occur, but more detailed analysis is required to map out these areas as functions of laser operating current [6].

The bistable or switching behaviour of the two-section laser amplifier has been used for optical time-division switching [7] and wavelength conversion [8]. Conversion between wavelengths of 1.3μm and 1.55μm has been achieved [9] using saturable absorber with a minimum switching power of 60mW. Further details of these and other applications of two-section lasers and amplifiers can be found in a recent review by Kawaguchi [10]. Wavelength conversion within the 1.55μm window using gain saturation in a single-section laser amplifier has been demonstrated [11], and further discussion of this will be given below in the section devoted to speed of response.

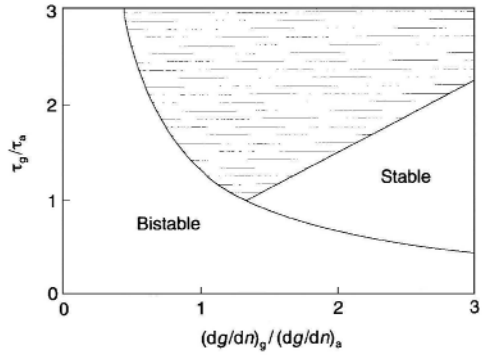

Fig.(2): Stability diagram for two-section devices; shaded area is the region where self-pulsations can occur

The self-pulsating behaviour of the two-section laser has been used for all-optical clock recovery [12]. When optical data is injected into the device, the clock component of the data locks the self-pulsations to the clock's phase and

frequency. Inspection of Equation 4 and Fig. 2 shows that the lifetime in the absorber section, τ_a, must be shorter than that in the gain section, τ_g, if a useful range of self-pulsation is to be achieved. This is particularly important in InGaAsP devices where Auger recombination causes a reduction of τ_g at high carrier concentrations. In order to reduce τ_a, this section of the device is selectively doped with a high concentration of zinc [13]. Control of the natural frequency of self-pulsation is achieved by variation of the drive current to the gain section, and clock recovery at rates up to 5Gbs^{-1} have been achieved [13]. For split-contact DFB lasers, higher natural frequencies of self-pulsation have been observed (up to 30GHz [14]), and the mechanism is attributed to the relative shift between feedback spectra for the two sections [15]. Further details of clock recovery using two-section devices can be found in the recent review by Barnsley [16].

2.3 Interband nonlinear refraction

Associated with the gain or absorption saturation discussed above, there is the corresponding process of nonlinear refraction. The change of refractive index with carrier concentration in a semiconductor laser contains contributions from the free carrier plasma effect [17] and the anomalous band-edge dispersion effect [18], with the latter usually dominant for most cases of interest. It is usually a good approximation to assume that the refractive index, N, varies linearly with carrier concentration for wavelengths near the band edge, and manipulation of the steady-state rate equations yields the following result for N as a function of optical power P:

$$N = N_0 - g_0\left(\frac{dN/dn}{dg/dn}\right)\frac{P/P_{sat}}{1+P/P_{sat}} \quad (5)$$

here N_0 is the value of refractive index in the absence of light, dN/dn is the derivative of the index with respect to carrier concentration, and the other quantities are as defined previously. The ratio dN/dn to dg/dn is directly proportional to the linewidth enhancement factor [19], which is widely used in studies of laser chirp. Typical values for InGaAsP at 1.55μm wavelength are dN/dn=-2x10^{-20}cm^{-3}, g_0=300cm^{-1}, dg/dn=2.5x10^{-16}cm^2, so that index changes as large as 0.02 can be achieved in principle for sufficiently high powers. Alternatively, a phase change of π should be achievable for P/P_{sat}=0.1 in a device of typical length around 400μm. Note that this power P is some mean value within the amplifier; therefore, in general, the measured input power will be considerably less than P.

To make use of the phase change available from a nonlinear amplifier, it is necessary to use a suitable interferometric configuration in order to effect a switching action. The simplest such configuration is the Fabry-Perot cavity occurring in an uncoated laser amplifier. The nonlinear phase change then acts to change the optical path length in the cavity and to shift the resonances to longer wavelength with increasing optical power. Thus, by tuning the input signal to the long-wavelength side of a Fabry-Perot resonance it is possible to observe nonlinearity and bistability in the plots of output versus detuning [20] and output versus input power [21]. For InGaAsP amplifiers biased just below lasing threshold, minimum switching powers are of order 1μW [22] with a switching time of about 1-10ps and a recovery time limited by the recombination lifetime to around 1ns [23,24].

When a nonlinear Fabry-Perot amplifier is operated in reflection rather than transmission, a particularly rich variety of bistable behaviour is predicted [25] and observed [26], as illustrated schematically in Fig. 3. For values of gain close to threshold (curve number 1 in Fig. 3) the hysteresis loop is traversed in an anticlockwise sense (as in the case for transmission), while for low values of gain (curve number 2) the loop is described in a clockwise sense (similar to that for reflection from a passive Fabry-Perot etalon); for intermediate values of gain X-shaped or butterfly hysteresis is found, as illustrated by curve 3 in Fig. 3. Bistability is also observed when an amplifier is operated above threshold [27] as an injection-locked laser, when recovery time is reduced to less than 100ps [28]. This mode of operation has recently been used to demonstrate all-optical switching, pulse reshaping and wavelength conversion at speeds to 10Gbs^{-1} [29].

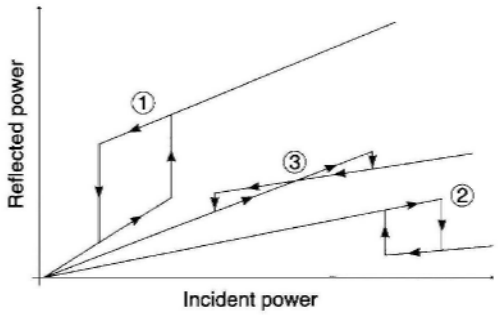

Fig.(3): Reflected power versus input power for an uncoated laser amplifier (schematic): 1, high gain (close to threshold); 2, low gain; 3, intermediate gain

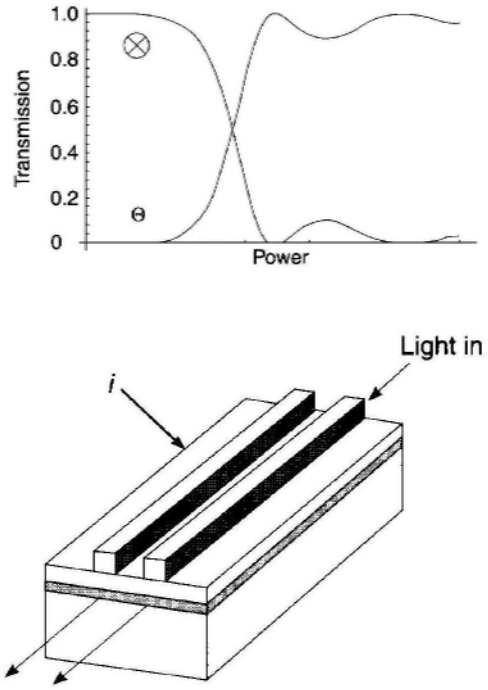

Fig.(4): Active nonlinear directional coupler, and its ideal switch characteristics

A second example of a configuration to exploit optically-induced phase changes is the nonlinear directional coupler [30]. The active version of this [31], consisting of two closely-spaced ridge-waveguide amplifiers, is shown schematically in Fig. 4. The device length is arranged such that for low input powers the output is in the cross state, whilst for sufficiently high powers the coupling is altered via the induced phase change so that the output switches to the through-state. The theoretical switching characteristics for steady state operation are also shown in Fig.4. Analysis of such a coupler has indicated that an input switching power of the order of milliwatts is required [32]. The corresponding analysis for ultrashort-pulse self-switching [33] indicates that the switching energy if of the order of picojoules, but that switching from the cross- to the through-state is limited to 50% of the output energy. A Fabry-Perot version of the device has been demonstrated experimentally [34] and shown to switch at input powers of the order of microwatts although it displays a strong sensitivity to input wavelength since its operation depends on optical feedback from the facets [35]. Pulsed measurements on a similar device [36] show partial switching with an input pulse energy of 60pJ coupled into the waveguide for 10ps pulses.

As a third example of the exploitation of nonlinear refraction in amplifiers, consider the loop mirror (Sagnac interferometer) configuration illustrated in Fig. 5. An incident pulse at one of the input terminals is split by the coupler to give clockwise and counterclockwise propagating components. With an amplifier and an attenuator in the loop, the two components generate different mean powers in the amplifier, and thus they experience different gain and phase changes. The pulses arrive back at the coupler simultaneously, interfere, and produce two outputs whose magnitudes depend on the phase difference between the two components. With this setup, self-routing of optical pulses has been demonstrated on 10ns pulses with powers of less than 250μW, within a 17m loop [37].

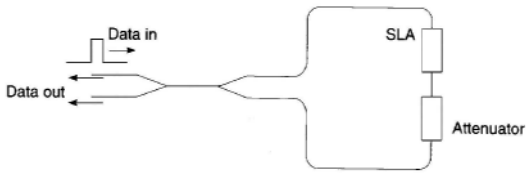

Fig.(5): Nonreciprocal loop mirror configuration (SLA=semiconductor laser amplifier)

The semiconductor laser amplifier in a loop mirror (SLALOM) configuration [38] is a similar concept to that discussed above and illustrated in Fig. 5, except that the attenuator is omitted and the amplifier is displaced from the center of the loop by a specified distance. This displacement result in a temporal delay between pulses arriving at the amplifier that can be used to perform a correlation operation [38]. The SLALOM has been used as a decision gate for all-optical data retiming with simultaneous wavelength translation over 60nm [39], as well as for pulse shaping and noise reduction in a recirculating fibre loop [40]. By comparison with conventional fibre loop mirror configurations that utilize several kilometers of fibre, the SLALOM has the advantage that it could be integrated on a single chip.

2.4 Speed of response

The dynamic properties of interband nonlinearities in laser amplifiers are governed (in a small-signal approximation) by the effective carrier lifetime, τ_{eff}, given by

$$\frac{1}{\tau_{eff}} = \frac{1+\dfrac{P}{P_{sat}}}{\tau_c} \qquad (6)$$

where τ_c is the differential carrier lifetime, i.e. $\tau_c=(\mathrm{d}R/\mathrm{d}n)^{-1}$, where R is the total recombination rate and n is the carrier concentration. Note that the differential lifetime

is two to three times lower than the static carrier lifetime, so that values for t_c will lie typically in the range 200-750ps, decreasing with increasing drive current [41]. Since the power P is the mean value in the amplifier, it may take values more than one order of magnitude greater than the input power, and hence reductions are possible in principle for input powers of a few milliwatts, say. This combination of high drive currents and moderate input optical powers has been used in a number of instances recently to effect faster response times from amplifiers than the nanosecond recombination time restriction that was previously assumed to apply. However, the optical power must be present either continuously or at a regular high frequency, so that the carrier population cannot recover to any significant extent from its saturation value.

The principle outlined above has been used to obtain fast response times for wavelength conversion using gain saturation in laser amplifiers [11, 42]. The data signal ('probe') channel and a CW ('pump') channel are input into the amplifier, so that the pump saturates the gain (as illustrated in Fig. 6) and is then modulated according to the bit pattern of the probe. The gain recovery time, which limits the response speed, can be shortened by using probe powers of a few milliwatts. Conversion has been demonstrated recently by this technique over wavelength ranges up to 17nm at bit rates of $10Gbs^{-1}$ [43] and $20Gbs^{-1}$ [44-46]. A potential problem with the technique is that the extinction ratio of the probe output is reduced. This can be avoided by using the phase shift experienced by the probe and using an interferometric technique to convert this to an amplitude modulation [44].

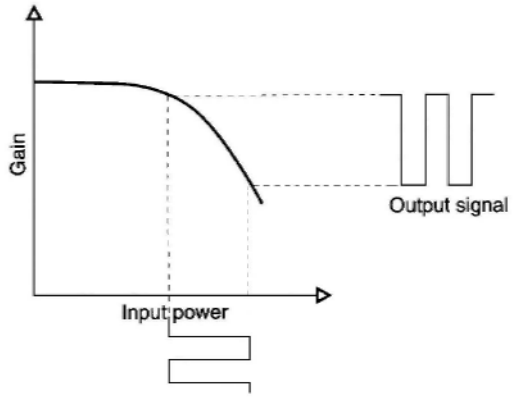

Fig.(6): Principle of operation of wavelength conversion by gain saturation

A further improvement may be offered by the use of third (CW) beam to speed up this response, thus allowing the probe powers to be reduced [45, 46]. The use of such a holding beam has been demonstrated to reduce the response time to around 10ps for an input power of 32mW ata bias of 300mA [48]. This configuration has also been used to achieve all-optical clock recovery at $20Gbs^{-1}$ using an amplifier as an intracavity mode-locking element in a mode-locked erbium-doped fibre ring laser [49]. It has also been proposed [47] that a holding beam could be employed for all-optical demultiplexing with the SLALOM [38] discussed earlier, in order to enhance the recovery rate of the amplifier to be faster than the clock rate.

Another approach to high-speed performance from nonlinear amplifiers is based on a configuration that utilizes only the fast switch-on response to an optical pulse, and thus avoids the recovery time associated with the slower switch-off time. Such a configuration is the terahertz optical asymmetric demultiplexer (TOAD) [50], illustrated schematically in Fig. 7. This differs from the SLALOM configuration in that an additional coupler is included in the loop so that a high-intensity control pulse can be arranged to pas through the loop. The signal pulse, which is of relatively low intensity, is split into clockwise (c.w.) and counterclockwise (c.c.w.) propagating components in the usual way (c.w. does not refer to 'continuous wave' in this context). When the control pulse passes through the amplifier, it creates a very fast (sub-picosecond) change in the gain and refractive index of the amplifier active material. If the amplifier is displaced a distance x from the center of the loop then the c.w. and c.c.w. pulses experience this index change separated by a time $2x/v$, where v is the speed of light in the loop, and both will experience the fast response characteristic of the nonlinearity switch-on time. The result is that the TOAD output exhibits a time-window of width $2x/v$ with profile characterized by rise and fall times of the order of picoseconds and a flat top (since the nonlinearity recovers on a nanosecond timescale). The only pulses that emerge from the loop's output are those within this window, so that the TOAD can be used to demultiplex pulses with bit period greater than or equal to $2x/v$. by incorporating a variable fibre delay in the loop [51, 52], the width of the time-window, and hence the maximum frequency for demultiplexing, can be varied.

Experimental demonstrations of all-optical demultiplexing using TOAD have been reported at bit rates of $40Gbs^{-1}$ [51], $50Gbs^{-1}$ [54]. In these examples the amplifier is allowed to completely recover between switching pulses, leading, for example, to a single-channel rate of $100Mbs^{-1}$ in [54]. Provided that the switching pulse train is a regular clock, there are no problems associated

with patterning, so the amplifier does not need to recover fully between switching pulses, and much higher channel rates are possible. In this manner a TOAD-like configuration has been used to demonstrate demultiplexing of a $10Gbs^{-1}$ channel from line rates of $40Gbs^{-1}$ [51] and $160Gbs^{-1}$ [52].

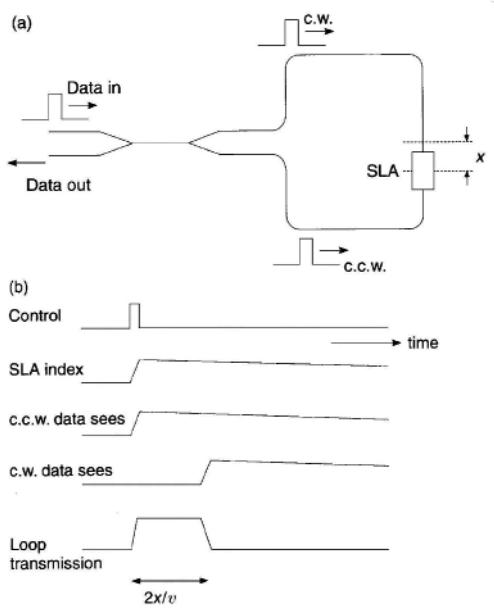

Fig.(7): Principle of operation of the TOAD: (a) configuration; (b) temporal responses

3. Intraband nonlinearities

For pulses whose width is much less than the carrier lifetime, the gain saturation is determined by the saturation energy, $E_{sat}=EA/(\Gamma dg/dn)$, with typical values of a few picojoules. Under these conditions the amplifier gain is independent of the pulsewidth [55, 56]. However, for sub-picosecond pulsewidth it is found experimentally that the saturation energy is no longer given by this simple expression and is dependent on pulsewidth [57]. This finding has been successfully explained [58] by a theoretical model that includes two intraband processes: carrier heating and spectral hole-burning. These processes affect the distribution of carriers in the energy bands but leave the overall carrier concentrations unchanged. For InGaAsP amplifiers, carrier heating has a time constant in the range 200-700fs, while spectral hole-burning is characterized by a time constant of 50-80fs. These values have been determined by comparing theory and experiment for pump-probe measurements on bulk [59, 60] and quantum-well [61, 62] amplifiers.

Ultrafast nonlinear refraction attributed to carrier heating and spectral hole-burning in amplifiers has been observed in measurements of self-phase modulation [63,64] and time-division interferometry [65, 66]. The time constants required to empirically fit the observed changes in refractive index are the same as those for the measured gain saturation, thus supporting the conclusion that the same mechanisms are responsible. The characteristic response function for the measured phase shift [65, 66] shows (1) an almost instantaneous portion attributed to a very rapid electronic or virtual process; (2) a contribution due to carrier heating that recovers with a time constant of order 1ps; and (3) the interband contribution with a nanosecond recovery time. For pulsewidths much shorter than 1ps, the index change ΔN is proportional to the peak pump pulse energy density ε_p (i.e. energy divided by area) and is given by $\Delta N/\varepsilon_p$=25 to 28 cm^2W^{-1} [66].

A particularly interesting case of interband nonlinearity occurs for amplifiers operated at the transparency current, since the long-lived interband nonlinearity disappears in this situation [63, 65]. The definition of transparency is illustrated in Fig. 8, and corresponds to zero net stimulated emission, where the photon energy is equal to the quasi-Fermi level separation. Thus for any given input wavelength it is possible to find a current at which the transparency condition is satisfied. Experimental results on bulk [63, 65] and quantum-well [67] amplifiers biased at transparency indicate an intensity-dependent refractive index with a nonlinearity coefficient of the order of $10^{-11}cm^2W^{-1}$, and that the index change may be regarded as instantaneous for pulsewidths of order 10ps. The details of the physical mechanism responsible are not yet clear, but intraband carrier dynamics are thought to be involved as well as a resonantly enhanced optical Stark effect [68]. The effect has been exploited in active directional couplers operated at transparency in both InGaAsP [69] and GaAs/AlGaAs [70]. In the former case, partial switching was achieved for 14ps pulses with 9W peak power, while in the latter device a switching crossover was achieved for input pulse energies of order 10pJ and pulsewidth 130fs.

Another situation where intraband effects are of special importance occurs in four-wave mixing in optical amplifiers. If two intense optical signals at different frequencies ν_1, ν_2 are injected into an amplifier, then a grating can be formed at the beat frequency between the signals. At frequency separations (ν_1-ν_2) up to few gigahertz, the grating is formed as a modulation in the carrier density and is characterized by carrier lifetime [71]. However, for wider frequency separations, the grating mechanism is nonlinear gain due to modulation of the

occupation probabilities of the carriers within an energy band, and is characterized by intraband response times [72]. Interactions of these types in semiconductor lasers were first analyzed [73] to explain the asymmetric gain saturation around a strong signal wave. The first experimental observation of nearly degenerate four-wave mixing (NDFWM) in a semiconductor laser above threshold [74] demonstrated that phase-conjugate signals at frequencies $(2\nu_1-\nu_2)$ and $(2\nu_2-\nu_1)$ could be generated with high efficiency for pump powers of only a few milliwatts. NDFWM was also observed in traveling-wave semiconductor amplifiers [75] and identified as a source of crosstalk in frequency-division multiplexed transmission [76, 77] as well as a potentially useful mechanism for frequency conversion [78].

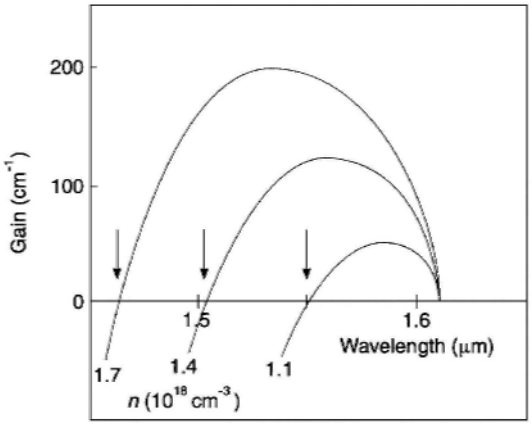

Fig.(8): Gain spectra for various currents (carrier concentrations), illustrating the definition of transparency (denoted by arrows)

Information on the nature of intraband nonlinearity responsible for NDFWM at high frequency separations has been obtained from experiments where the separation is extended to 500GHz [79] and beyond 1THz [80, 81] ('highly nondegenrate four-wave mixing' HNDFWM). An example of the frequency response for phase-conjugate signals in a 1.5μm laser amplifier is given in Fig. 9. This curve has been calculated by assuming a carrier density modulation characterized by a lifetime of 0.1ns, and a carrier temperature modulation characterized by a response time of 0.5ps. Fitting curves of this type to experimental data [79-81] reveals intraband time constants of 500-650fs, consistent with carrier heating effects.

The use of NDFWM for frequency conversion is limited to frequency separations below about 5GHz by the efficiency (see Fig.9). In order to enlarge this frequency spacing, a second pump beam has been used to generate further sidebands [82], resulting in a conversion range of 4000GHz. Another way to achieve a large frequency range is the use of cavity enhancement effects when the pump and signal beams coincide with Fabry-Perot resonances of an uncoated laser amplifier. This technique has resulted in 1THz frequency translation of a 1Gbs^{-1} intensity-modulated signal with a bit error rate (BER) of 10^{-9} for a power penalty of 1dB [83]. A third means to obtain a wide range of frequency conversion with high efficiency is to use an AR-coated amplifier in strong saturation with high saturated gain [84]. Measurements indicate that the conversion efficiency (defined as the ratio of wavelength-converted output power to coupled signal input power) increases with the saturated gain and would reach values in excess of 100% if the gain could be 19dB [84]. This technique has been used to obtain a 10^{-9} BER at 622Mbs^{-1} with a power penalty of 1.1dB for wavelength conversion over 2.5THz [84]. BER measurements have also been reported [85] for 500GHz frequency-converted signals at bit rates of 1, 2.5, 5 and 10Gbs^{-1}.

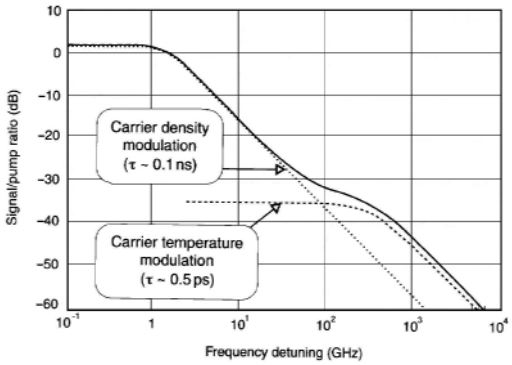

Fig.(9): Ratio of conjugate to pump beam intensity for a traveling-wave amplifier

Another useful property of the four-wave mixing process is that the phase-conjugate beam is spectrally inverted with respect to the input signal. This effect forms the basis for a novel method of dispersion compensation in long-distance fibre links [86]. A laser amplifier positioned midway along a fibre link is used to spectrally invert the signal so that the effects of dispersion accumulated in the first half of the transmission are exactly reversed in the second half. This has been demonstrated experimentally by transmission of a highly chirped 2.5Gbs^{-1} signal at 1.5μm across 100km of standard fibre with only 0.9dB penalty at 10^{-9} BER [87], and of a 10Gbs^{-1} signal over 200km with 0.7dB penalty at 10^{-9} BER [88].

4. Conclusion

The nonlinearities occurring in semiconductor laser amplifiers have sometimes been seen as obstacles to the achievement of efficient linear amplification of optical signals. However, these nonlinearities also have the potential for generating new functionality when exploited in appropriate amplifier configurations. This review has attempted to highlight these newer applications and to focus on the underlying physical mechanisms responsible for the nonlinearities. In this way the limitations on power, speed and other parameters have been addressed and recent spectacular achievements set in the context of prior work. The topic of nonlinear applications of laser amplifiers is currently very active and it I anticipated that there is scope for considerable further progress in the relatively near future.

References

[1] M.J. Adams *et al.*, *IEEE J. Quantum Electron.*, QE-21 (1985) 1498.
[2] G.J. Lasher, *Solid State Electron.*, 7 (1964) 707.
[3] N.G. Basov, *IEEE J. Quantum Electron.*, QE-4, (1968) 856.
[4] H. Kawaguchi, *Electron. Lett.*, 17 (1981) 741.
[5] M. Ueno and R. Lang, *J. Appl. Phys.*, 58 (1985) 1689.
[6] M.J. Adams *et al.*, *unpublished results.*
[7] S. Suzuki *et al.*, *J. Lightwave Technol.*, 4 (1986) 894.
[8] H. Kawaguchi *et al.*, *Electron. Lett.*, 23 (1987) 1088.
[9] P.E. Barnsley and P.J. Fiddyment, *IEEE Photon. Technol. Lett.*, 3 (1991) 256.
[10] H. Kawaguchi, *IEE Proc. J*, 140(1993) 3.
[11] B. Glance *et al.*, *Electron. Lett.*, 28 (1992) 1714.
[12] M. Jinno and T. Matsumoto, *Electron. Lett.*, 24 (1988) 1426.
[13] P.E. Barnsley *et al.*, *IEEE Photon. Technol. Lett.*, 3 (1991) 942.
[14] B. Sartorius *et al.*, *European Conference on Optical Communications*, 1993, paper WeP8.2, p.365.
[15] U. Bandelow, H.J. Wunsche and H. Wenzel, *IEEE Photon. Technol. Lett.*, 5 (1993) 1176.
[16] P. Barnsley, *IEE Proc. J*, 140 (1993) 325.
[17] A.K. Jonscher and M.H. Boyle, *Proc. IPPS Symposium on GaAs*, 1966, p.78.
[18] G.H.B. Thompson, *Opto-electronics*, 4 (1972) 257.
[19] C.H. Henry, *IEEE J. Quantum Electron.*, QE-18 (1982) 259.
[20] K. Otsuka and S. Kobayashi, *Electron. Lett.*, 19 (1983) 262.
[21] T. Nakai, N. Ogasawara and R. Ito, *Jpn J. Appl. Phys.*, 22 (1983) L310.
[22] W.F. Sharfin and M. Dagenais, *Appl. Phys. Lett.*, 46 (1985) 819.
[23] M.J. Adams, *IEE Proc. J*, 132 (1985) 343.
[24] H.J. Westlake, M.J. Adams and M.J. O'Mahony, *Electron. Lett.*, 22 (1986) 541.
[25] M.J. Adams, *Opt. Quantum Electron.*, 19 (1987) S27.
[26] N.F. Mitchell *et al.*, *Opt. Lett.*, 19 (1994) 269.
[27] H. Kawaguchi *et al.*, *IEEE J. Quantum Electron.*, QE-21 (1985) 1314.
[28] R. Hui *et al.*, *Opt. Lett.*, 18 (1993) 1733.
[29] K. Welch, E. Patzak and J. Horer, *Electron. Lett.*, 30 (1994) 493.
[30] S.M. Jensen, *IEEE J. Quantum Electron.*, QE-18 (1982) 1580.
[31] C.J. Setterlind and L. Thylen, *IEEE J. Quantum Electron.*, QE-22 (1986) 595.
[32] J.M. Liu and C. Yeh, *Appl. Phys. Lett.*, 50 (1987) 1625.
[33] S. Trillo *et al.*, *IEEE J. Quantum Electron.*, QE-27 (1991) 410.
[34] D.A.H. Mace *et al.*, *Electron. Lett.*, 25 (1989) 987.
[35] M.J. Adams *et al.*, *IEEE J. Quantum Electron.*, QE-26 (1990) 1764.
[36] C.L. Chuang *et al.*, *Int. J. Nonlinear Opt. Phys.*, 1 (1992) 799.
[37] A.W. O'Neill and R.P. Webb, *Electron. Lett.*, 26 (1992) 2008.
[38] M. Eiselt, *Electron. Lett.*, 28 (2992) 1505.
[39] M. Eiselt, W. Pieper and H.G. Weber, *Electron. Lett.*, 29 (1993) 107.
[40] M. Eiselt *et al.*, *IEEE Photon. Technol. Lett.*, 5 (1993) 422.
[41] N. Storkfelt *et al.*, *IEEE Photon. Technol. Lett.*, 3 (1991) 632.
[42] C. Joergensen *et al.*, *IEEE Photon. Technol. Lett.*, 5 (1993) 657.
[43] J.M. Wiesenfeld *et al.*, *IEEE Photon. Technol. Lett.*, 5 (1993) 1300.
[44] B. Mikkelsen *et al.*, *Proc. European Conference on Optical Communications*, 1993, paper ThP12.6, p.73.
[45] D.M. Patrick and R.J. Manning, *Electron. Lett.*, 30 (1994) 252.
[46] J.M. Wiesenfeld *et al.*, *Electron. Lett.*, 30 (1994) 720.
[47] R.J. Manning and D.A.O. Davies, *Opt. Lett.*, 19 (1994) 889.
[48] R.J. Manning *et al.*, *Electron. Lett.*, 30 (1994) 787.
[49] D.M. Patrick and R.J. Manning, *Electron. Lett.*, 30 (1994) 151.

[50] J.P. Sokoloff *et al.*, *IEEE Photon. Technol. Lett.*, 5 (1993) 787.
[51] A.D. Ellis and D.M. Spirit, *Electron. Lett.*, 29 (1993) 2115.
[52] K. Suzuki *et al.*, *Electron. Lett.*, 30 (1994) 660.
[53] J.P. Sokoloff *et al.*, *IEEE Photon. Technol. Lett.*, 6 (1994) 98.
[54] I. Glesk, J.P. Sokoloff and P.R. Prucnal, *Electron. Lett.*, 30 (1994) 339.
[55] G.P. Agrawal and N.A. Olsson, *IEEE J. Quantum Electron.*, 25 (1989) 2297.
[56] T. Saitoh and T. Mukai, *IEEE J. Quantum Electron.*, 26 (1990) 2086.
[57] Y. Lai *et al.*, *IEEE Photon. Technol. Lett.*, 2 (1990) 711.
[58] A. Uskov, J. Mork and J. Mark, *IEEE Photon. Technol. Lett.*, 4 (1992) 443.
[59] K.L. Hall *et al.*, *Appl. Phys. Lett.*, 56 (1990) 1740.
[60] J. Mark and J. Mork, *Appl. Phys. Lett.*, 61 (1992) 2281.
[61] K.L. Hall *et al.*, *Appl. Phys. Lett.*, 61 (1992) 2512.
[62] M. Willatzen *et al.*, *Appl. Phys. Lett.*, 64 (1994) 143.
[63] R.S. Grant and W. Sibbett, *Appl. Phys. Lett.*, 58 (1991) 1119.
[64] P.J. Delfyett, Y. Silberberg and G.A. Alphonse, *Appl. Phys. Lett.*, 59 (1991) 10.
[65] C.T. Hultgren and E.P. Ippen, *Appl. Phys. Lett.*, 59 (1991) 635.
[66] K.L. Hall *et al.*, *Appl. Phys. Lett.*, 62 (1993) 1320.
[67] M.A. Fisher *et al.*, *Electron. Lett.*, 29 (1993) 1185.
[68] M. Sheik-Bahae and E.W. van Stryland, *Proc. QELS'92*, Anaheim, 1992, paper QThD19, p.228.
[69] D.A.O. Davies *et al.*, *Electron. Lett.*, 29 (1993) 1710
[70] S.G. Lee *et al.*, *Appl. Phys. Lett.*, 64 (1994) 454.
[71] G.P. Agarwal, *Opt. Lett.*, 12 (1987) 260.
[72] G.P. Agarwal, *Appl. Phys. Lett.*, 51 (1987) 302.
[73] AP. Bogatov, P.G. Eliseev and B.N. Sverdlov, *IEEE J. Quantum Electrn.*, QE-11 (1975) 510.
[74] H. Nakajima and R. Frey, *Appl. Phys. Lett.*, 47 (1985) 769.
[75] K. Inoue, T. Mukai and T. Saitoh, *Appl. Phys. Lett.*, 51 (1987) 1051.
[76] K. Inoue, *Electron. Lett.*, 23 (1987) 1293.
[77] R.M. Jopson *et al.*, *Electron. Lett.*, 23 (1987) 1394.
[78] G. Grosskopf *et al.*, *Electron. Lett.*, 24 (1988) 31.
[79] L.F. Tiemeijer, *Appl. Phys. Lett.*, 59 (191) 499.
[80] M.C. Tatham, G. Sherlock and C.P. Seltzer, *Proc. Quantum Optoelectronics Topical Meeting*, Palm Springs, 1993, paper QWD4-1, p.46.
[81] J. Zhou *et al.*, *Appl. Phys. Lett.*, 63 (1993) 1179.
[82] G. Grosskopf, R. Ludwig and H.G. Weber, *Electron. Lett.*, 24 (188) 1106.
[83] S. Murata *et al.*, *IEEE Photon. Technol. Lett.*, 3 (1991) 1021.
[84] M.C. Tatham, G. Sherlock and L.D. Westbrook, *IEEE Photon. Technol. Lett.*, 5 (1993) 1303.
[85] R. Ludwig and G. Raybon, *Electron. Lett.*, 30 (1994) 338.
[86] A. Yariv, D. Fekete and D.M. Pepper, *Opt. Lett.*, 4 (1979) 52.
[87] M.C. Tatham, G. Sherlock and L.D. Westbrook, *Electron. Lett.*, 29 (1993) 1851.
[88] M.C. Tatham *et al.*, *Electron. Lett.*, 30 (1994) 1335.

SYMPOSIA
ON OPTICS AND OPTICAL TECHNOLOGY

SPIE International Symposium Optifab
North America's Premier Optical Fabrication Exhibition
2 - 5 May 2005
Rochester, NY USA
Advance Registration Ends at 15 April 2005

SPIE Europe International Symposium Optical Metrology
13 - 16 June 2005 (Abstracts Due 20 December 2004)
Munich, Germany

XII Joint International Symposium on Atmospheric and Ocean Optics/Atmospheric Physics
27 - 30 June 2005
Tomsk, Russia
Sponsored by SPIE Russia Chapter. SPIE will publish proceedings.

SPIE Europe International Symposium on Optical Systems Design
12 - 16 September 2005 (Abstracts Due 28 February 2005)
Jena, Germany
Exhibition

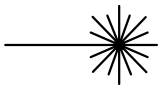

Boulder Damage Symposium XXXVII
Annual Symposium on Optical Materials for High Power Lasers
19 - 21 September 2005 (Abstracts Due 31 May 2005)
Boulder, CO USA
Abstract submissions will be accepted starting in mid February

SPIE Europe Symposium Optics/Photonics for Defence & Security
26 - 29 September 2005 (Abstracts Due 11 April 2005)
Bruges, Belgium (Exhibition)

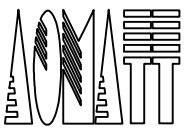

The Second International Symposium on Advanced Optical Manufacturing and Testing Technologies (AOMATT)
2 - 5 November 2005
Xian, China
SPIE is a technical cosponsor and will publish the proceedings

Salwan K. Al-Ani [1]
Raid A. Ismail [2]
Hana F. Al-Ta'ay [2]

[1] *Faculty of Education, Seyoun-Hadhramout University, YEMEN, Email: salwan_kamal@yahoo.com*
[2] *Physics Science and Research Center, Ministry of Science and Technology, Baghdad, IRAQ*

Characterization of CdS:In/Si Heterojunction Solar Cells

In this work, CdS:In/Si anisotype heterojunction solar cells prepared by thermal evaporation technique of CdS thin films on monocrystalline silicon substrate have been fabricated, characterized and analyzed. Cells aparameters dependencies on the indium diffusion temperature were reported. The amximum obtained conversion efficiency was 8% at 93mW/cm^2 (AM1) for cells made with indium diffusion temperature of 300°C. these cells are made without using antireflecting coatings and grid contacts.

Keywords: *CdS:In, Solar cells, Anisotype heterojunction, Diffusion temperature*

Received: 3 August 2004, Revised: 10 December 2004, Accepted: 15 January 2005

1- Introduction

There has been considerable interest in recent years directed toward the development of heterojunction solar cell. Such attention is based on the fact that heterojunction devices have a number of advantages over diffused p-n junction devices some of these advantages include [1]:

1. Lower costing fabrication
2. Lower junction formation temperature
3. Higher spectral response at short wavelengths (λ=300-600nm)
4. Many of deposited layers have indices of refraction to act as antireflection coating.
5. Window effect taken place in heterojunction reduces the role of surface recombination effect.

In order to increase the conversion efficiency of a heterojunction solar cell, the energy gap of the base material should lie in the range (1.1-1.9)eV. The window material should have as large a gap as possible and the lattice mismatch as well as the difference in electron affinity between the two materials should be a minimum [2]. CdS has proved to be one of the best materials for window applications in heterojunction type solar cell [3.4]. To enhance the photovoltaic properties of CdS/Si solar cells Coluzza et al. prepared CdS:In/Si solar cells by co–evaporation technique and efficiency of 8% have been obtained [5]. In this paper we report a study of electrical and photovoltic properties of heterojunction In-doped n-CdS/p-Si solar cells which have been prepared by thermal diffusion. On the other hand, comparison with undoped CdS/Si solar cells have been presented.

2- Experiment

Glass and p-type (111) single crystal silicon wafers were used as substrates. The resistivity and thickness of silicon wafers were (1-5 Ω.cm) and (500±50μm), respectively. One of these wafers was polished. Prior to deposition of CdS film, these wafers were chemically etched in dilute hydrofluoric acid to remove native oxides, then back contact metallization was accomplished by depositing 200nm of aluminum in vacuum. After removed from the vacuum chamber, the wafers were scribed into individual pieces of 0.5cm^2 sizes where they are ready for the CdS deposition.

The deposition of CdS films was carried out by thermal evaporation in vacuum (~10^{-6} torr) onto a 100°C-heated silicon substrates. Indium-doped CdS/Si heterojunction solar cells were achieved using the following procedure.

Indium of high purity (99.999%) was evaporated onto the CdS film in vacuum. The deposited In layer of thickness ~20nm was thermally diffused into the CdS using a vacuum furnace in the temperature range (T_d= 200-350)°C. The top metal electrode was then formed by depositing 200nm Al through a metal mask. The sensitive area was 0.2cm^2. The Optical transmittance of CdS films was measured using UV-VIS-PV-8800 spectrophotometer in the wavelength range (300-900)nm.

Current–Voltage (I-V) measurements were performed on different sample with different parameters. The voltage applied to the specimen from stabilized DC power supply was slowly increased from zero up to (3V) for the forward

bias connection. The voltage across sample and the current passing through it were measured using electrometers of type (KEITHLY-616 Digital).

Capacitance–Voltage (C-V) measurement in the reverse bias voltage (0-3)V and frequenies of (1MHz) were done using *hp/4192 ALF* LCZ system. The I-V illumination measurements were done a different illumination power densities (22-120)mW/cm^2 supplied by a 120W PHILLIPS halogen lamp, which is connected to a variac and calibrated by a silicon powermeter. The I-V illumination was achieved under simulated AM1 condition (93mW/cm^2). The samples were connected to a resistance box varied from to 10kΩ. Current and voltage were measured through this variation range.

3-Results and Discussion

3-1 Optical Measurements

The Transmittance spectra of CdS and CdS:In films as a function of wavelength are presented in Fig.(1). CdS film exhibits high transparency (~70%) at λ=550nm (the absorption edge of CdS is 2.4eV). This indicates that CdS acts as a window in the visible region when it is deposited on Si wafer whereas the CdS film doped with 2% In and submitted to different diffusion temperatures (T_d~(200-350)°C) has lower transmittance as T_d is increased and the absorption edge shifts towards longer wavelength (~11.5% at λ=600nm for CdS:In film at T_d =300°C). At T_d=350°C the transmittance starts to increase again. This is interpreted as follows: at high T_d, more In will be diffused into CdS film creating donor levels inside the energy gap and the fermi level will move towards the conduction band. The absorption of material increases at longer wavelength and causes a shift in the absorption edge [6-7].

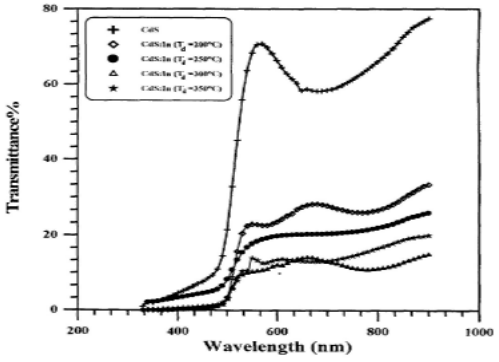

Fig. (1) Variation of transmittance as a function of wavelength for pure CdS and In-doped CdS at different diffusion temperatures

3-2 I-V Measurement in the Dark

A semi log(I-V) plot in the forward bias is presented in Fig.(2). This figure shows that forward current consists of two regions. The first one represents the recombination current, while the second region represents the tunneling current, i.e., CdS/Si and CdS:In/Si heterojunction obeys the tunneling–recombination model this result is in full agreement with results obtained by other workers [8-9].

The saturation current of the first region I_{s1} is determined by extrapolating (I-V) curve of this region to find its intercept at V=0 thus, the ideality factor (n) is calculated by the following equation [10-11]:

$$n = \frac{q}{KT}\frac{\partial v}{\partial \ln(I_{f_1}/I_{s1})} \qquad (1)$$

where q/KT is the reciprocal of the volt equivalent of temperature, I_{f1} is the forward current for the recombination region and I_{s1} is the saturation current for this region.

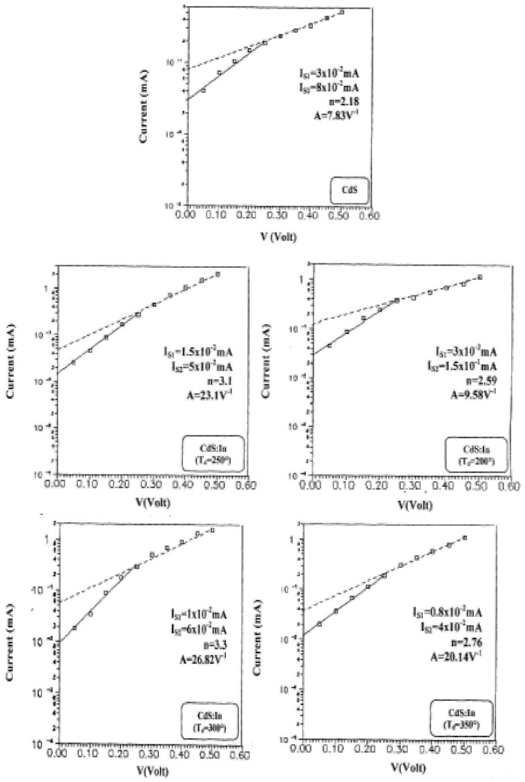

Fig. (2): Forward I-V characteristics for anisotype heterojunction pure CdS and In-doped CdS

On the other hand, the saturation current of the second region I_{s2} is determined by the extrapolation of the second region then value of (A) is extracted by the following equation [10]:

$$A = \frac{d \ln(I_{f2} / I_{S2})}{dv} \qquad (2)$$

where I_{f2} is the forward current for the tunneling region.

The values of A obtained in this paper agrees with result of other work [3].

3-3 Capacitance-Voltage Measuements

Figure (3) shows the reciprocal of square capacitance versus bias voltage ($1/C^2$-V). This plot shows a linear relationship with bias voltage and indicates that the junction is abrupt. This result is in full agreement with other work [9,12-13]. Also built–in potential (V_{bi}) can be calculated as explained before by extrapolating ($1/C^2$-V) plot to (($1/C^2$)=0) [14]. Table (1) shows values of V_{bi} calculated for CdS/Si and CdS:In/Si solar cells prepared at different T_d values.

Table (1) Built–in potential for n-CdS/p-Si and n-CdS:In/p-Si anisotype heterojunctions

Cells	V_{bi} (V)
CdS	2.29
CdS:In (T_d=200°C)	1.61
CdS:In (T_d=250°C)	1.50
CdS:In (T_d=300°C)	1.25
CdS:In (T_d=350°C)	2.00

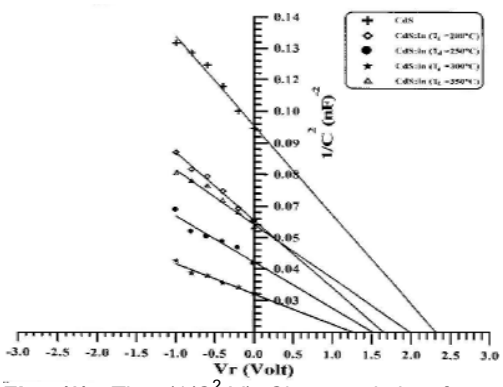

Fig. (3): The ($1/C^2$-V) Characteristics for pure cells and doped at different diffusion temperatures

3-4 Photovoltaic Measurements

Figure (4) and (5) show the open circuit voltage (V_{oc}) and short circuit current density (J_{sc}) as functions of incident optical power density on the solar cell. An increase in J_{sc} and V_{oc} with different illuminating power densities is observed. Those figures exhibited a good photovoltaic performance due to anisotype heterojunction formation [15].

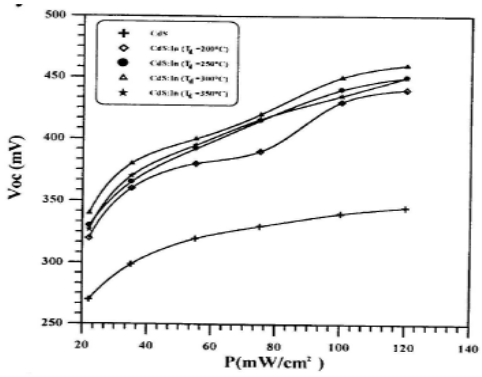

Fig. (4): Variation of V_{oc} as a function of illumination power density for CdS and CdS:In heterojunctions prepared at different T_d values

The behavior of the cell is linear at the beginning due to increase the incident photon flux. A saturation state occurs with increase of the power density in a certain range due to the recombination process, which depends on the current density through the depletion layer.

Figure (6) displays variation of the V_{oc} and J_{sc} with In diffusion temperature at a power density 93mW/cm^2. The increase in the values of V_{oc} and J_{sc} is attributed to the best condition of In diffusion in CdS film.

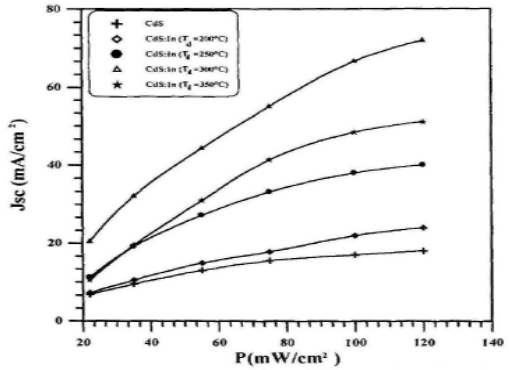

Fig. (5): Variation of J_{sc} as a function of illumination power density for pure heterojunctions prepared at different T_d values

3-5 Solar Cell Parameters

Figure (7) shows variation of the output power density versus the voltage through load resistance of the pure and doped cells. The highest conversion efficiency was 3% for pure CdS solar cell. For CdS:In at T_d=300°C the maximum efficiency have been obtained was 8% without using grid frontal electrode and antireflection coating.

Figure (8) shows the maximum output power of heterojunction cell which is normally lower than homogenous p-n junction due to the surface recombination effects and the lattice mismatch in

CdS/Si junction. Table (2) presents the parameters of these photovoltaic cells.

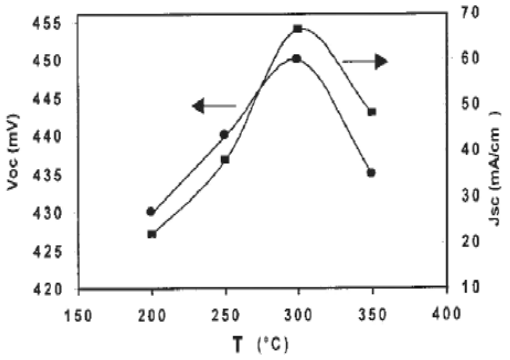

Fig. (6): Variation of the short–circuit current density (J_{sc}) and open–circuit voltage (V_{oc}) with diffusion temperature at irradiance of 93mW/cm^2

Table (2) ***Photovoltaic parameters of n-CdS/p-Si and n-CdS:In/p-Si Cells under AM1 Illumination***

Cell	J_{sc} (mA/cm^2)	V_{oc} (mV)	F.F	η%
CdS/Si	18.5	380	0.42	3.192
CdS:In (200°C)	23	460	0.34	3.888
CdS:In (250°C)	38.66	400	0.26	4.346
CdS:In (300°C)	66.66	400	0.3	8.647
CdS:In (350°C)	48	440	0.32	7.306

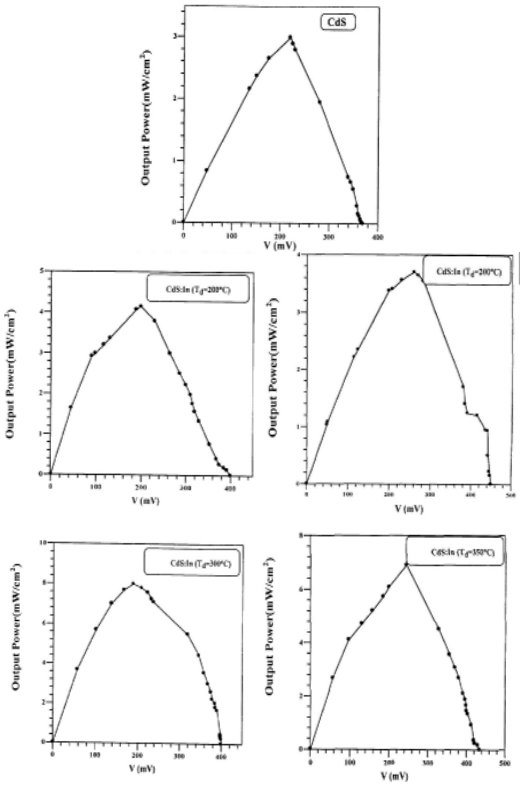

Fig. (7): Variation of the output power density for CdS/Si and CdS:In/Si heterojunction solar cells

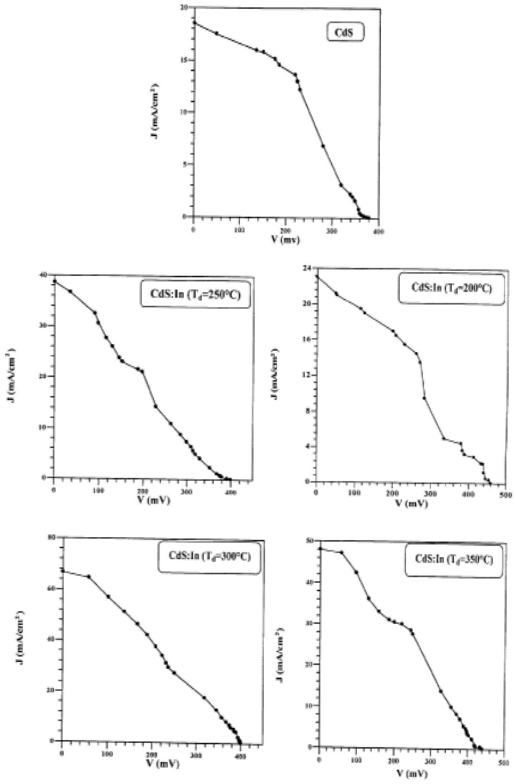

Fig. (8): Photovoltaic performance of CdS/Si and CdS:In/Si heterojunctions solar cells under simulated AM1 (93mW/cm^2)

4. Conclusions

The CdS/Si heterojunction prepared by thermal evaporation and CdS:In/Si prepared by different thermal diffusion temperatures are suitable to fabricate high efficient solar cells with a conversion efficiency of about 3% for pure CdS solar cells and 8% for CdS:In/Si solar cells. This is because of the window effect taken place between these combinations which reduces the role of surface recombination effects. The forward current of this junction obeys tunneling–recombination model and (C-V) measurements revealed that n-CdS/p-Si and n-CdS:In/p-Si heterojunctions are abrupt.

References

[1] T. Feng, A.K. Gosh and C. Fishman, *Appl. Phys. Lett.*, Vol.35, No.3, 1979, 266-268.

[2] F.A. Abou Elfotouh, R.Al-Wadi and M. Abo-Elnaby, *Thin Solid Films*, Vol.96, 1982, 169-173.

[3] E. Cigdem and B. Murat, *Solar Cells*, Vol.26, 1989, 253-262.

[4] H. Okimura, M. Kawakami and Y. Sukai, *Jpn. J. Appl. Phys.*, Vol.6, 1967, 908.

[5] C. Coluzza, M. Garozzo and Tomaciello, *Appl. Phys. Lett.*, Vol.37, No.6, 1980, 569-572.
[6] S. Major and A. Banergec, *Thin Solid Films*, Vol.122, 1984, 31.
[7] P.C. Mathur, B.R. Sethi and O.P. Sharma, *J. Appl. Phys.*, Vol.52, No.12, 1981, 7237.
[8] R.A. Ismail, A.E. Al-Samar'ai and O.A.A. Sultan, *Iraqi J. Al-Rafidain Eng.*, Vol.8, No.2, 2000, 77-83.
[9] E. Cigdan and B. Murat, *Solar Cells*, 26 (1989) 253.
[10] B.L. Sharma and R.K. Puroit, "**Semiconductor Heterojunction**", Pergamon Press (NY), 1974, p. 42.
[11] A. Georgakilas, E. Aperathitis and P. Panayotates, *Mater. Sci. Eng.*, Vol.B44, 1997, 383-386.
[12] H. Tashiya, T. Nishikura and Y. Ema, *Jpn. J. Appl. Phys.*, Vol.28, No.7, 1989, 1174-1177.
[13] H. Okimura and R. Kondo, *Jpn. J. Appl. Phys.*, Vol.9, No.3, 1970, 274-280.
[14] S. Dengyuan, Z. Jianua and A. G. Aterle, **17 European Photovoltaics Conference** (Munich) (2001), p. 116.

WORKSHOPS

Ninth International Workshop on
Nondestructive Testing and Computer Simulations
6 - 12 June 2005
St. Petersburg, Russia
Sponsored by SPIE Russia Chapter.
SPIE will publish proceedings.

Workshop on Building European OLED Infrastructure
6 - 7 June 2005
Cambridge, United Kingdom
Abstracts Due 3 April 2005

The 5th International Workshop on
Adaptive Optics for Industry
and Medicine
29 August - 2 September 2005
Beijing, China
SPIE is a cooperating organization and will publish proceedings

MEETINGS

SPIE Europe Regional Meeting Opto Ireland
4 - 6 April 2005
Dublin, Ireland
Advance Registration Ends at 18 March 2005

Optics & Photonics 2005
co-located with the ***SPIE 50th Annual Meeting***
San Diego, California USA
31 July - 4 August 2005 (Exhibition)
Abstracts Due 17 January 2005

Saratov Fall Meeting 2005
26 - 30 September 2005
Saratov, Russia
Sponsored by SPIE Russia Chapter. SPIE will publish proceedings.

Annual Meeting of the Federation of Analytical Chemistry and Spectroscopy Societies (FACSS 2005)
9 - 13 October 2005
Quebec City, Canada
SPIE is a cooperating organization

SEMINARS

Seventh Seminar on
Problems of Theoretical and Applied Electron and Ion Optics
25 - 27 May 2005
Moscow, Russia
Sponsored by SPIE Russia Chapter.
SPIE will publish proceedings.

Bulk Properties of $YBa_2Cu_3O_7$ Superconducting Materials

Dayah N. Raouf

School of Applied Sciences
University of Technology,
Baghdad, IRAQ, Email:
dnraouf2005@yahoo.com

In this paper, bulk properties of high-temperature superconducting (HTSC) $YBa_2Cu_3O_7$ (YBCO) material have been studied at a dominant orthorhombic phase, which represents more than 90% of the structure. These properties included x-ray diffraction pattern, unit cell parameters, hardness, porosity, density, transition temperature, breakdown voltage, and finally possibility of drilling holes in the disc pellet of HTSC ceramic material.

Keywords: *Superconductors, HTS, YBCO, Bulk properties*

Received: 19 October 2004, Revised: 4 December 2004, Accepted: 5 December 2004

1. Introduction

The discovery of HTSC ceramic materials by Bednorz and Muller in 1986[1] has brought the possibility of superconductor applications at liquid nitrogen temperature such as loop antenna [2], microstrip antenna [3], Josephson junctions [4], transmission lines [5], coils [6], squid [7], and wires [8]. These applications and others require a knowledge of the properties of HTSC materials. In this work, the preparation and characterization of bulk HTSC YBCO material which has a dominant (>90%) orthorhombic phase has been carried out.

2. Experiment

A pellet disc of HTSC $YBa_2Cu_3O_{7-\delta}$ material has been prepared by the standard solid-state reaction technique [9]. Initially, stoichometric weights of a dry, research grade powders of Y_2O_3 (99.999%), $BaCO_3$ (99.99%) and CuO (99.9%) were mixed up together and ground to a fine powder by a gate mortar and pestle for a period of 3 hours. The gray-colored pulverized powder was placed into high purity (99.8%) alumina boat. The latter was placed inside a quartz tube where the boat was centered at the hot zone of a homemade tube furnace. The powder was calcinated for an accumulated time of 48 hours in 6 equal-time intervals, at temperature of 920°C in oxygen gas flow. The calcinated black powder then re-ground again to a fine powder using a gate mortar for 2 hours. The pulverized powder was then compressed into pellet disc by applying 7 tons of hydrostatic pressure onto 1.25cm-diameter die. These pellets were sintered at temperature range between 950-960°C for 18 hours in oxygen gas flow. The temperature was measured by R-type platinum 13% rhodium/platinum thermocouple wires. The pellets were quenched from ~960°C to room temperature by natural (air) cooling.

3. Results and Discussion

Initially, the pellets were tested as a superconductor by Mizner effect where the pellet was connected to a fine thread and then immersed in liquid nitrogen, then brought close to a permanent magnet. A big repulsion, between the pellet and the magnet, had been noticed which indicates that the material becomes paramagnetic whereas no repulsion was noticed before the cooling process. This means that the material was diamagnetic material.

Table (1): d_{hkl} values extracted from ASTM and calculated from Fig. (1)

d (ASTM)	d (calculated)	I/I_o	hkl
3.890	3.880	12	010
2.749	2.740	46	013
2.728		82	103
2.331	2.323	20	014
2.233	2.234	18	113
1.945	1.940	67	020
1.911	1.914	14	200
1.583	1.582	100	123

The transition temperature (T_c) was measured, to be 95K±1K, by a non-contact method [13-14] using a K-type nickel-chromium/copper-nickel thermocouple wire.

The X-ray phase analysis was carried out by x-ray diffraction using Phillips x-ray diffractometer with vertical goniometer employing a radiation source Fe(k_α) of

λ=1.937Å and Mn filter. The diffraction intensity versus 2θ for the YBCO material is shown in Fig. (1). The d_{hkl}-spacing was calculated from $d_{hkl}sin\theta=n\lambda$, and the results were compared with the d_{hkl}-spacing from ASTM. It was in good agreement and they are tabulated in Table (1).

The results indicate that the $YBa_2Cu_3O_7$ compound has a ratio of >90% dominant orthorhombic phase. Also, there is a little ratio of copper oxide (CuO) and some traces of impurities like Y_2O_5 and Ba_2O.

The unit cell parameters, a, b and c, were calculated from the following relation:

$$d_{hkl} = \frac{1}{[(\frac{a}{h})^2 + (\frac{b}{k})^2 + (\frac{c}{l})^2]^{\frac{1}{2}}} \quad (1)$$

giving the cell parameters as: a=0.3828nm, b=0.388nm and c=1.16097nm, where they were calculated for the 010, 200 and 013 indices which agree with the literature within 99.23% [11]. Also, they indicate that it is orthorhombic and the O_2 content is $6<\delta<7$ [11].

The surface morphology was studied using an optical microscope and presented in Fig. (2). The surface shows two phases: the first (dominant) is orthorhombic phase, as supported by x-ray diffraction, and the second is the porous which is estimated by measuring the relative area of porosity for few sections. The results were then averaged and found to be about 14.47%.

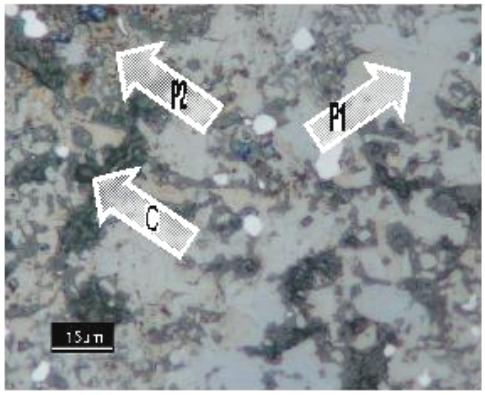

Fig. (2) Surface morphology using optical microscope shows two phases p_1 , p_2 and porosity c

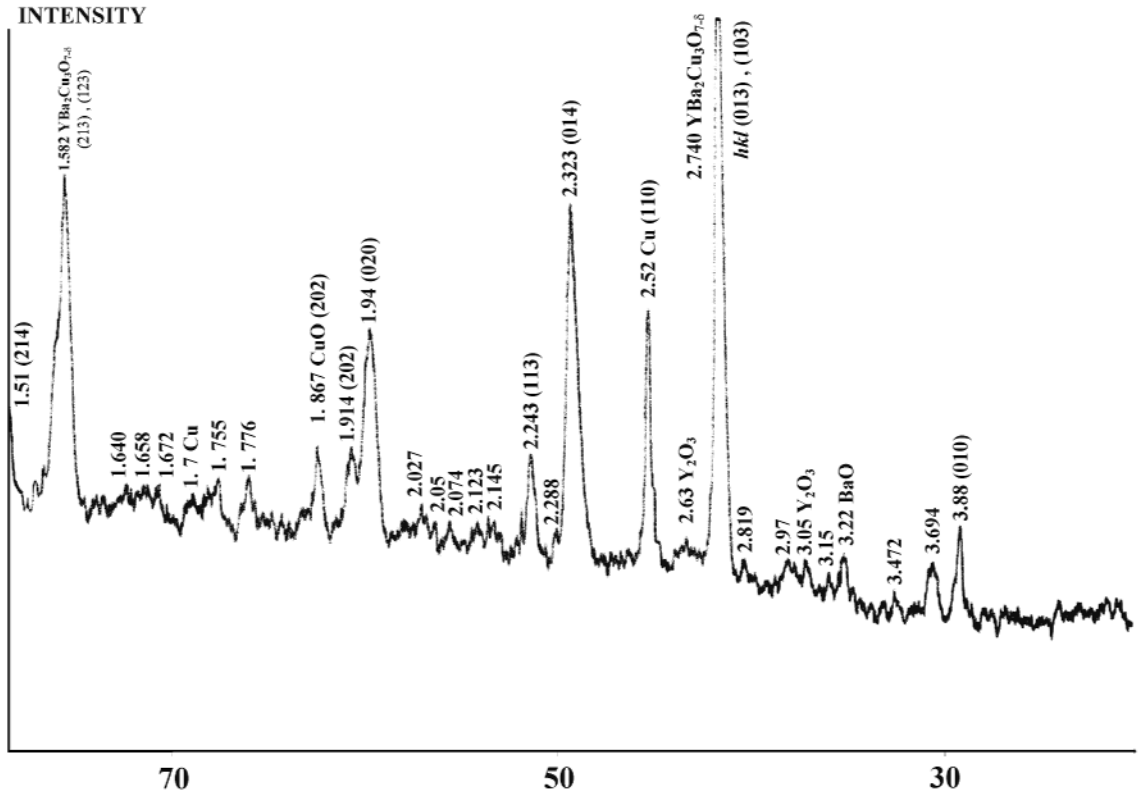

Fig. (1) X-ray diffraction pattern: intensity vs. 2θ

The hardness of the YBCO was measured by supporting the brittle bulk material by PVC as in Fig. (3a). the fixed surface was polished and then tested by Brinell method. The hardness was calculated from the following relation [12]:

$$Bhn = \frac{2P}{\pi D(D - \sqrt{D^2 - d^2})} \qquad (2)$$

where the load applied P=0.102kg, ball diameter D=2.5mm and indentation diameter d=1.06nm (Fig. (3b)), giving Bhn=110.13kgf. Although, it may be lower because the surface morphology of the sample in Fig. (3b) shows some filamentary cracks in the material.

The density of the YBCO material was calculated after the extraction of the porosity volume from the bulk volume and giving a density (fused) value of 5.9g.cm^{-3}, which is in close agreement with the theoretical (X-ray density) value of 6.3 [11]. Such range of density is a good indication that the dominant phase is the orthorhombic.

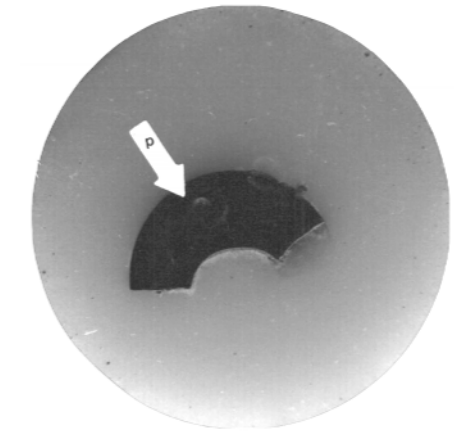

(a)

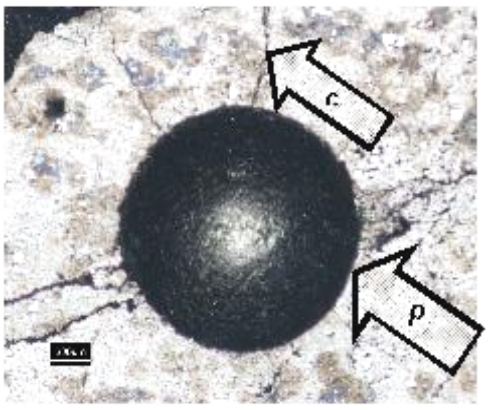

(b)

Fig. (3) (a) Supported HTS (black) by PVC (grey) (b) Magnified pit (*p*) surrounded by filamentary cracks (*c*)

It is found that it is very simple to drill a hole in a solid disc of the YBCO material as shown in Fig. (4). However, the disc must first be glued on a piece of wood carefully, and then followed by the drilling process. Although it looks simple, it is reducing a lot of complication by making dies to shape the produced superconductor with certain holes in it. A range of holes where tested from 1mm to 5.8mm in diameter on a 1.25cm-diameter and 0.35cm-thickness pellet.

The breakdown voltage for the superconductor disc was found to be 1.972kV/cm, although, when a rating voltage of 0.5kV/s is initially used, a field of ~1.12kV/cm was noticed. This is attributed to the situation that the material behaves as semiconductor at room temperature.

Also, it was noticed that the sample accepts compression of $\Delta L \approx 0.027$ at load of 1.3kN before failure limit as shown in Fig. (5) where the relation is linear.

Fig. (4) HTS disc where the hole diameter is 5.8mm

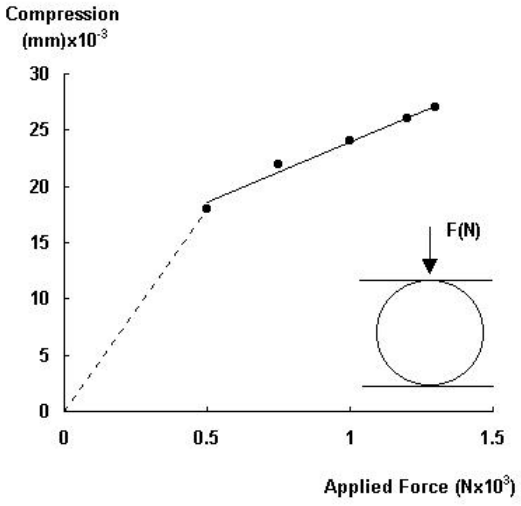

Fig. (5) Compression vs. applied force on the YBCO material of 1.25cm diameter and 0.355cm thickness

4. Conclusions

Although the orthorhombic phase >90% appears by x-ray analysis, the traces of impurities are due to the inhomogeneous powder mixing process. The YBCO 123 phases are critical to temperature and this explains the appearance of other phases. It is noticed that the drilling of the YBCO ceramic is quite easy since the bulk YBCO has a good compressibility of the material. The leakage field indicates that the material is semiconductor at room temperature.

Acknowledgment

The author would like to thank the following people for using their labs and their support during the work. They are Dr. B. M. Dhiaa, Miss. K. S. Khashan, Mrs. N. Al-Darzy, Dr. S. S. Abdul-Noor, Dr. K. T. Rasool and Mrs. F. A. Saeed.

References

1. Bednorz, J. G. and Műller, K. A., *J. Phys. B*, Vol.64, 1986, p.189.
2. Wang, J., Leigh, J. Jr., Wicklund, S. and Stein, A., *Supercond. Sci. Technol*., Vol.1, 1988, p.24.
3. Gűney, K., *ELEKTRIK*, Vol.1, No.3, 1993, p.193.
4. Peterson, R. L. and Ekin, J. W., *Phys. Rev. B*, Vol.37, No.16, 1988, p.9848.
5. Sakai, S., *Phys. Rev. B*, Vol.36, No.1, 1987, p.812.
6. Lusk, M., Lund, J., Chaklader, A., Burkant, M., Fife, A., *Supercond. Sci. Technol*., Vol.1, 1988, p.137.
7. Pagano, S. and Barone, A., *Supercond. Sci. Technol.*, Vol.10, 1997, p.904.
8. Jin, S., Sherwood, R., van Dover, R., Tiefel, T. and Johnson, D. Jr., *Appl. Phys. Lett*., Vol.51, No.3, 1987, p.203.
9. Mei, Y. and Luo, H. L., *J. Appl. Phys*., Vol.64, No.5, 1988, p.2533.
10. Ramadan, A. A., Abdel-Hady, S., Abdel-Ghany, S. and Soltan, S. E., *Egypt. J. Solid*., Vol.23, No.1, 2000, p.59.
11. Hanic, F., Cigan, A., Buchta, S., Manka, J. and Jrubec, V., *Measur. Sci. Rev*., Vol.1, No.1, 2001, p.45.
12. Lakhtin, Y., "**Engineering Physical Metallurgy**", MIR Publishers (MOSCOW), 1977, p.78.
13. Boss, J. D. et al., *Rev. Sci. Instrum*., Vol.59, No.4, 1988, p.659.
14. Raouf, D. N., Al-Sharify, F. and Ahmed K. A., *J. College Education* (Published in Iraq), Vol.5, 2001, p.19.

CONFERENCES

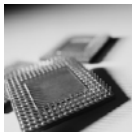

Photomask Japan 2005
13 - 15 April 2005
Yokohama, Japan
Advance Registration Ends at 24 March 2005

IS&T Archiving Conference 2005
26 - 29 April 2005
Alexandria, Virginia USA
SPIE is a cooperating organization

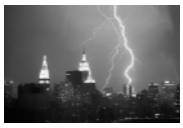

ICONO 2005: International Conference on Coherent and Nonlinear Optics co-located with LAT 2005: ***International Conference on Lasers, Applications, and Technologies***
11 - 15 May 2005 St. Petersburg, Russia
Sponsored by SPIE Russia Chapter. SPIE will publish proceedings.

Holography 2005 International Conference on Holography, Optical Recording, and Processing of Information
21 - 25 May 2005 Varna, Bulgaria
Sponsored by SPIE Bulgaria Chapter. SPIE will publish proceedings.

17th International Conference on Optical Fibre Sensors
23 - 27 May 2005
Bruges, Belgium
SPIE is a cooperating organization and will publish proceedings

XVIth Conference on Photonics and Web Engineering
31 May - 5 June 2005
Wilga Resort, Poland
Organized by SPIE Poland Chapter, SPIE Student Branch-WUT and IEEE Poland section. SPIE will publish proceedings

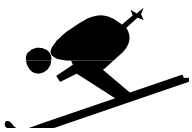

Lasers for Measurement and Information Transfer 2005
8 - 10 June 2005
St. Petersburg, Russia
Sponsored by SPIE Russia Chapter. SPIE will publish proceedings.

European Conference on Biomedical Optics
13 - 16 June 2005
Munich, Germany
SPIE is co-sponsor with OSA

EOS Conference on Industrial Imaging and Machine Vision
13 - 16 June 2005
Munich, Germany
SPIE is a cooperating organization
Abstracts Due 28 February 2005

10th OptoElectronics and Communications Conference (OECC 2005)
5 - 8 July 2005
Seoul, South Korea
SPIE is a technical cosponsor

Visual Communications and Image Processing (VCIP 2005)
12 - 15 July 2005
Beijing, China
SPIE is a cooperating organization

ICOXX-20th Congress of the International Commission for Optics
21 - 26 August 2005 Changchun, China
SPIE is a cosponsor.

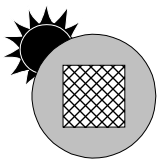

International Congress on Optics and Optoelectronics
28 August - 2 September 2005
Warsaw, Poland
Sponsored by SPIE Europe and SPIE Polish Chapter (Exhibition)
Abstracts Due 14 February 2005

Fourth Pacific Rim Conference on Photonics and Imaging in Biology and Medicine (PIBM 2005)
3 - 6 September 2005 Tianjin, China
SPIE is a cooperating organization and will publish proceedings

Seventh International Conference on Correlation Optics
6 - 9 September 2005 Chernivtsi, Ukraine
Sponsored by SPIE Ukraine Chapter and SPIE Russia Chapter.
SPIE will publish proceedings.

Photonics North 2005
12 - 14 September 2005 Toronto, Canada
Cosponsored by SPIE and Canadian Photonics Consortium.
Abstracts Due 28 March 2005 (Exhibition)

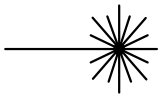

Atomic and Molecular Pulsed Lasers
12 - 16 September 2005
Tomsk, Russia
Sponsored by SPIE Russia Chapter.

PECS 2005: Photon Echo and Coherent Spectroscopy
18 - 25 September 2005
Kaliningrad, Russia

Micro- and Nanoelectronics 2005
co-located with ***Quantum Informatics 2005***
3 - 7 October 2005 Moscow, Russia
Sponsored by SPIE Russia Chapter. SPIE will publish proceedings.

International Conference on
Control and Synchronization of Dynamical Systems
4 - 7 October 2005
Leon, Guanajuato Mexico
SPIE is a cooperating organization

Optics East
23 - 26 October 2005
Boston, MA USA (Exhibition)
Abstracts Due 11 April 2005

ETOP 2005 Conference on
Education and Training in Optics and Photonics
23 - 27 October 2005
Marseille, France
Sponsored by SPIE, OSA and ICO

The 6th International Young Scientists Conference
"Optics of High Technology Material Science"
27 - 30 October 2005
Kyiv, Ukraine
Sponsored by SPIE/Ukraine and OSA/Ukraine
Abstracts Due 15 June 2005

Optical Technologies for Communications 2005
28 - 30 November 2005
Ufa, Bashortostan Republic, Russia
Sponsored by SPIE Russia Chapter. SPIE will publish proceedings.

International Conference on
Optics & Optoelectronics-ICOL 2005
12 - 15 December 2005
Dehradun, India
SPIE is a cooperating organization

SYMPOSIA

SPIE Europe International Symposium
Microtechnologies for the New Millennium
9 - 11 May 2005
Sevilla, Spain
Advance Registration Ends at 25 April 2005

SPIE International Symposium Fluctuations and Noise
24 - 26 May 2005
Austin, Texas USA
Advance Registration Ends at 12 May 2005

SPIE Europe International Symposium on Remote Sensing
19 - 22 September 2005
Bruges, Belgium
Abstracts Due 21 March 2005
Exhibition

25th SPIE International Symposium Photomask Technology
3 - 7 October 2005
Monterey, California USA
Abstracts Due 18 April 2005
Exhibition

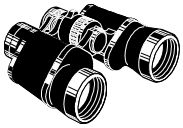

The Fourth International Symposium on Multispectral Image Processing and Pattern Recognition (MIPPR)
31 October - 2 November 2005
Wuhan, China
SPIE is a Technical Cosponsor and will publish the proceedings.

International Symposium APOC 2005
Asia-Pacific Optical Communications
6 - 10 November 2005
Shanghai, China
Abstracts Due 9 May 2005

Raid A. Ismail [1]
Walid K. Hamoudi [2]
Yasmeen Z. Daood [3]

[1] *Physics Science and Research Center, Ministry of Science and Technology, Baghdad, IRAQ,,* raidismail@yahoo.com
[2] *School of Applied Sciences, University of Technology, Baghdad, IRAQ*
[3] *Solar Energy Research Center, Ministry of Industry and Minerals, Baghdad, IRAQ*

Band Diagram of p-PbTe/n-Si Heterostructure

In the present work, the energy band diagram of p-PbTe/n-Si heterojunctions made by thermal evaporation of a polycrystalline PbTe layer deposited on a monocrystalline Silicon substrate is constructed. Based on I-V and C-V measurements, the band offsets ΔE_C and ΔE_V are found experimentally to be 270mV and 610mV respectively at 300K.

Keywords: *PbTe/Si thin films, Heterojunctions, Energy band diagram*

Received: 16 August 2004, Revised: 8 March 2005, Accepted: 15 March 2005

1. Introduction

Heterojunction devices have drawn a great attention in recent years mainly due to their use in the optoelectronic fields [1]. The properties of these heterojunctions are of critical importance when they are used as field-effect transistors (FET), bipolar transistor, light-emitting diode or lasers [2-3].

PbTe on Si structures are used for IR readout and imaging applications [4]. There is some work that has been reported on PbTe/Si heterojunctions where lattice mismatch is quite large. It has been shown that the preparation of the overlay layer plays an important role in the junction quality [5]. Hot-wall epitaxy (HWE) growth is a promising method to grow PbTe; it is clean and mostly reproducible.

Recently we have succeeded in fabricating a good quality PbTe/Si heterojunction using thermal evaporation technique [6]. In this paper, the band line-up of anisotype PbTe/Si heterojunction based on experimental results of I-V and C-V data was constructed. These results are compared with those for PbTe/Si heterojunction prepared by the HWE technique.

2. Experimental Details

Single crystal, 500μm thick n-Si wafers with resistivity of (1-3)Ω.cm were used as substrates. They were etched with dilute HF for about 10min in running hot deionized water and then dried. High purity 50 nm thick PbTe was deposited on cold Si substrates using a thermal resistance technique with pressure lower than 10^{-7} mbar. X-ray diffraction (XRD) analysis was performed using CuK_α radiation to confirm the crystalline structure of the PbTe layer. The conductivity type and sheet resistance of the PbTe films were investigated using Hall and four point probe measurements respectively.

Ohmic contacts were made on both, PbTe and Si, by deposition of In and Al, respectively. After contacts and assembly processes I-V (with different operating techniques) and C-V (10kHz) characteristics of the heterojunctions were investigated.

3. Results and Discussion

Fig. (1) shows an XRD spectrum of the PbTe films without post-deposition annealing. It is clear that the film is polycrystalline. Four peaks are observed in the pattern and can be indexed to the structure of PbTe with lattice constant of 0.645 nm. No diffraction peak corresponding to elements of Pb and Te were detected in any of our samples. Hall measurements confirm that PbTe and hence an anisotype heterojunction was formed.

A C-V characteristics of the heterojunction is shown in Fig. (2). It shows a straight line (abrupt junction) plot where $1/C^2=0$ points to the value of the built-in-voltage (V_D) according to the equation [7]:

$$V_D = V_{\text{int}} + \frac{2KT}{q} \qquad (1)$$

was calculated to be 0.6V. This is higher than the theoretical value, possibly due to the large degree of lattice mismatch (18%).

Fig. (3) depicts the dark I-V curve of the heterojunction at 300K. By applying the equation [3]:

$$n = \frac{KT}{q} . \frac{\Delta V}{\ln \frac{I_P}{I_S}} \qquad (2)$$

where KT/q is thermal voltage, I_S saturation current, the ideality factor (n) was deduced by Eq.(2) to be 1.6. This shows a mixed generation-recombination and diffusion current [8].

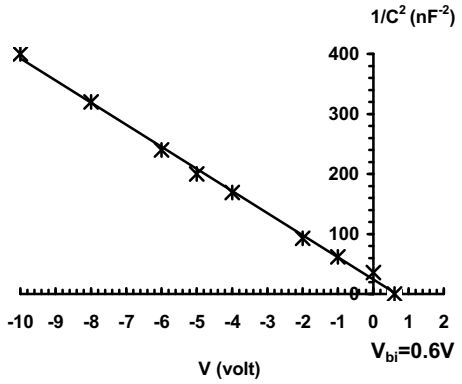

Fig. (2) $1/C^2$ with reverse bias voltage

Fig. (4) shows the semi-log scale of the temperature dependent I-V curves of the heterojunction. At lower temperature <298K no measurable current was noticed due to the exponential decrease of the current concentration at lower temperatures. From the I-V-T curves, the saturation currents were calculated and plotted as a function of ($1/T$) (Fig. 5).

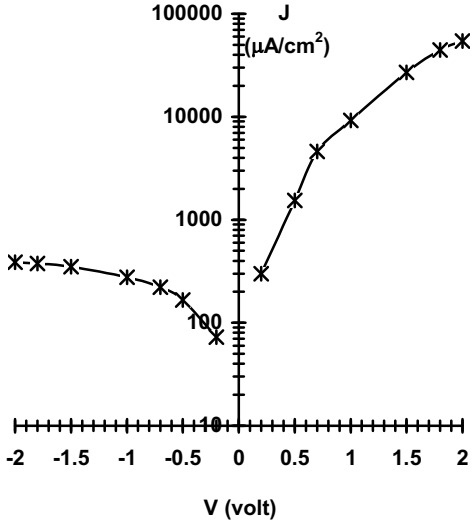

Fig. (3) Current-voltage characteristics for p-PbTe/n-Si anisotype heterojunction

The value of valence band offset ΔE_V was deduced from the slope of Fig. (5) using the

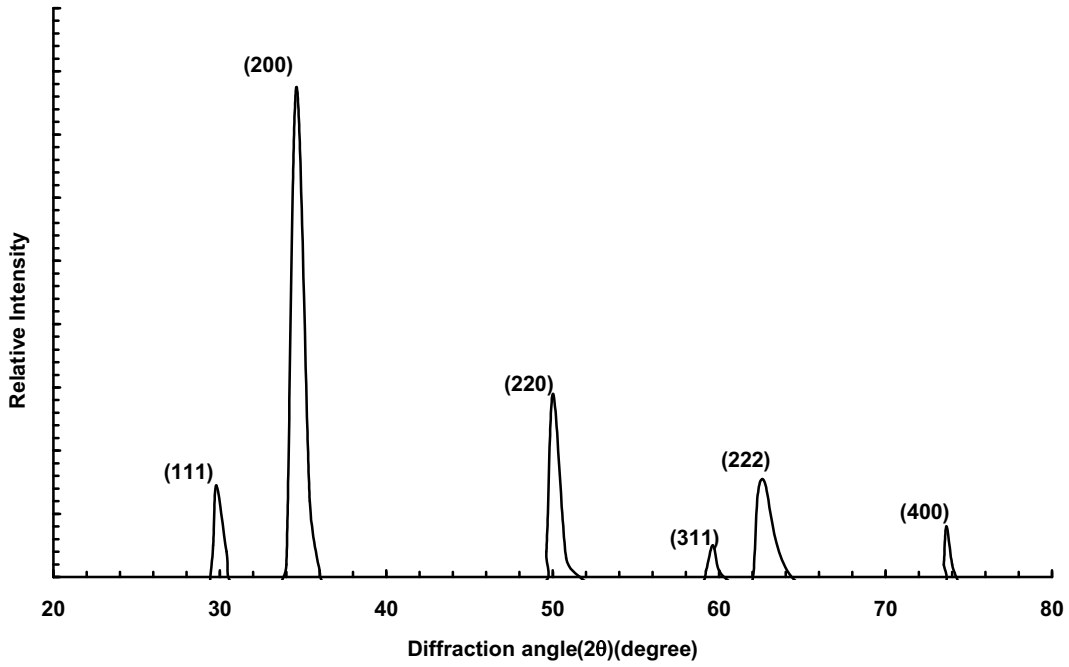

Fig. (1) X-ray diffraction spectrum of PbTe films

following equation [9,10]:

$$J_S = A\exp\left[\frac{-q(V_D - \Delta E_V)}{KT}\right] \qquad (3)$$

ΔE_V was found to be 610meV where A is constant.

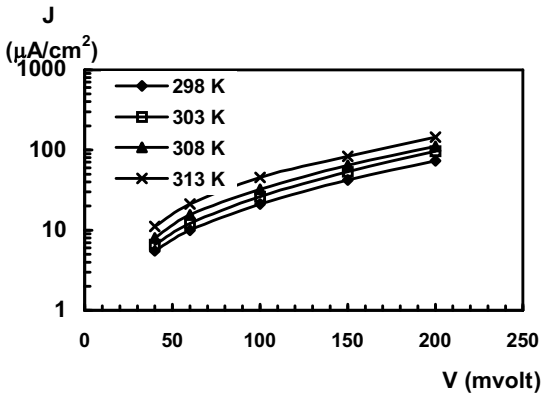

Fig. (4) Forward current density (J) against voltage (V) at temperatures between 298K and 313K

After inserting the band gap values for PbTe (0.30 eV) and for Si (1.11 eV), ΔE_C was calculated to be around 210meV. These values of band offset are slightly different from those reported by Vaya *et al.* [11]. This is attributed to the role of the preparation method of the PbTe layer. Fermi levels in PbTe (E_{fp}) and in Si (E_{fn}) were calculated and hence the energy band diagram was constructed and presented in Fig. (6). It is obvious from the band diagram that the band bending occurs only on the wide band gap (Si) while the bands remain flat in the PbTe side. This result is in good agreement with the result obtained by Vaya *et al.*

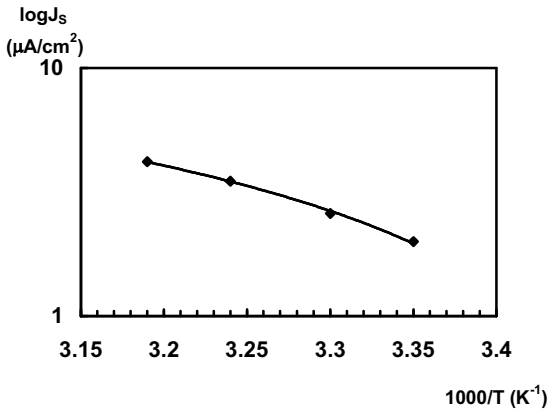

Fig. (5) J_S versus 1000/T for determination ΔE_V

The value of the conduction band offset ΔE_C was determined using the formula [8]:

$$\Delta E_C = E_g(Si) - E_g(PbTe) - \Delta E_V \qquad (4)$$

4. Conclusions

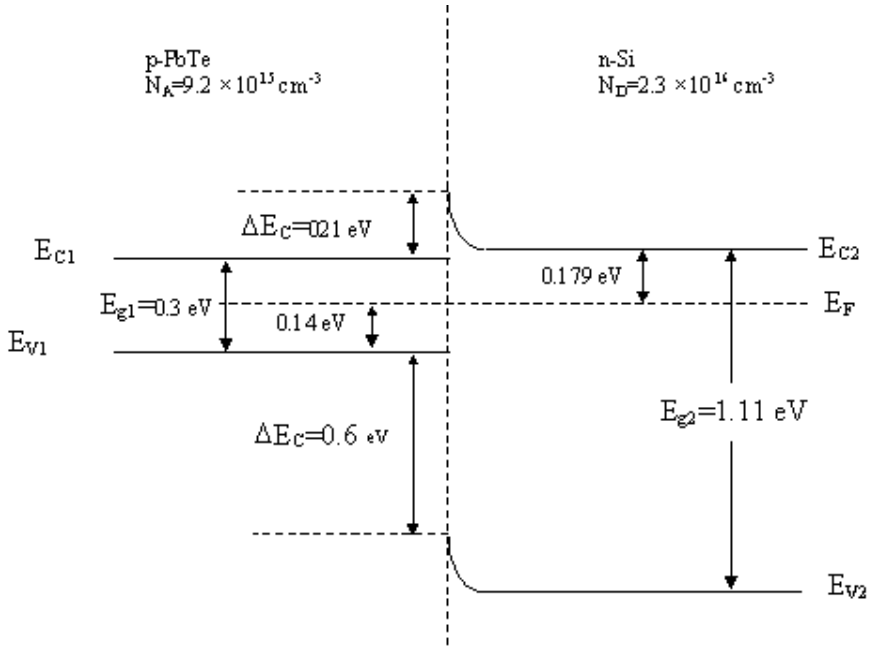

Fig. (6) Energy band diagram for p-PbTe/Si heterojunction

The band line-up of anisotype PbTe/Si heterojunction was constructed with the aid of I-V and C-V characteristics at 300K. The band diagram shows that despite the high resistivity of the deposited PbTe layer the PbTe/Si heterojunction behaves like a simple Schottky barrier device.

References

[1] R.A. Ismail and M.S. Mohammad, *J. Eng. Tech.* (Iraq), Vol.19 (2000).
[2] S.M. Potrous, *J. Eng. Tech.*, Vol.15(6) (1996), pp. 40-43.
[3] Zh.I. Alferov, "**Semiconductor Heterostructures: Physical Processes and Applications**", MIR Publishers (Moscow), (1989).
[4] K. Alchalabi, D. Zimin and H. Zogg, *IEEE Electron. Device Lett.*, Vol.3 (2001), pp.110-112.
[5] D.A. Neamen, "**Semiconductor physics and Devices**", McGraw-Hill (New York), (1992).
[6] W.K. Hamoudi, R.A. Ismail and Y.Z. Daood, *J. Eng Tech.* (Iraq), Vol.23(5) (2004), pp. 236-245.
[7] B. Sapoval and C. Hermann, "**Physics of Semiconductors**", Springer-Verlag (New York) (1995).
[8] S. Fujita, T. Yodo and A. Sasaki, *J. Cryst. Growth*, Vol.72 (1985), pp. 27-30.
[9] P.R. Vaya, J. Majhi, B.S.V. Gopalam and C. Dattatreynan, *Phys. Stat. Sol. (a)*, Vol.93(1) (1986), pp. 355-360.
[10] A. Georgakilas, E. Aperathitis, V. Foukaraki, M. Kayambaki and P. Panayotatos, *Mater. Sci. Eng.*, Vol.B44 (1997), pp. 383-386.
[11] V. D. Das and K. S. Bhat, *J. Appl. Phys.*, Vol.22 (1989), pp.126-168.

IRAQI JOURNAL OF APPLIED PHYSICS

" INSTRUCTIONS TO AUTHORS "

A new Iraqi specialized quarterly periodical dedicated to publishing original papers and letters in:

Applied & Nonlinear Optics
Applied Mechanics & Thermodynamics
Digital & Optical Communications
Electronic Materials & Devices
Laser Physics & Applications
Plasma Physics & Applications
Quantum Physics & Spectroscopy
Semiconductors & Optoelectronics
Solid State Physics & Applications

CONTRIBUTIONS

Contributions to be published in this journal should be original research works, i.e., those not already published or submitted for publication elsewhere, individual papers or letters to editor.

SUBMISSION OF MANUSCRIPTS

Manuscripts should be submitted to the editor at the mailing address:

Iraqi Journal of Applied Physics
Managing Editor
P. O. Box 55259, Baghdad 12001, IRAQ
irq_appl_phys@yahoo.com

Iraqi Journal of Applied Physics
Editor-In-Chief
P. O. Box 55159, Baghdad 12001, IRAQ
editor_ijap@yahoo.com

MANUSCRIPTS

Two copies with soft copy on a 3.5" diskette should be submitted to Editor in the following configuration:

- **Double-spaced one-side A4 size with 2.5 cm margins of all sides**
- **12pt Times New Roman font**
- **Letters should not exceed 5 pages, papers no more 20 pages and reviews are up to author.**
- **Manuscripts presented in English only are accepted.**
- **Authors confirm affiliations, addresses and emails. Email is necessary for correspondences.**
- **English abstract not exceed 150 words**
- **4 keywords (at least) should be maintained on (PACS preferred)**
- **Author(s) should express all quantities in SI units**
- **Equations should be written in equation form (italic and symbolic)**
- **Figures and Tables should be separated from text**
- **Figures and diagrams can be submitted in colors for assessment and they will be returned to authors after provide printable copies**
- **Charts should be indicated by the software used for**
- **Only original or high-resolution scanner photos are accepted**
- **References are written in titles, full-name authors, names of publications, years, volumes, issues and pages (from-to)**

PROOFS

Authors will receive proofs of papers and are requested to return one corrected hard copy with a WORD copy on a 3.5" diskette. New materials inserted in the original text without Editor permission may cause rejection of paper.

COPYRIGHT FORM

Author(s) will be asked to transfer copyrights of the article to the Journal soon after acceptance of it. This will ensure the widest possible dissemination of information.

OFFPRINTS

Authors will receive offprints free of charge and any additional offprints can be ordered.

SUBSCRIPTION AND ORDERS

Annual fees (4 issues per year) of subscription are:

- **36 000 Iraqi dinars for individuals and establishments inside Iraq.**
- **50 US$ for individuals and establishments abroad.**

Orders of issues can be submitted by contacting the editor-in-chief or editorial secretary to maintain the address of issue delivery and payment way.

THE IRAQI JOURNAL OF APPLIED PHYSICS
EDITORIAL BOARD
P. O. Box 55259, Baghdad 12001, IRAQ
Email: editor_ijap@yahoo.com

COPYRIGHY RELEASE

Iraqi Journal of Applied Physics (*IJAP*)

We, the undersigned, the author/authors of the article titled

……

……

that is presented to the Iraqi Journal of Applied Physics (IJAP) for publication, declare that we have neither taken part or full text from any published work by others, nor presented or published it elsewhere in any other journal. We also declare transferring copyrights and conduct of this article to the Iraqi Journal of Applied Physics (IJAP) after accepting it for publication.

The authors will keep the following rights:

1. Possession of the article such as patent rights.
2. Free of charge use of the article or part of it in any future work by the authors such as books and lecture notes without referring to the IJAP.
3. Republishing the article for any personal purposes of the authors after taking journal permission.

To be signed by all authors:

Signature:……..date: ……..

Printed name: ……..

Signature:……..date: ……..

Printed name: ……..

Signature:……..date: ……..

Printed name: ……..

Correspondence address:

……

……

Telephone:……Fax:……..email: …….

Note: Please complete and sign this form and mail it to the below address with your manuscript

The Iraqi Journal of Applied Physics,
P. O. Box 55259, Baghdad 12001, IRAQ
Email: irq_appl_phys@yahoo.com or editor_ijap@yahoo.com
Mobile: 07901274190